2-24-2021

Cellular and molecular dynamics during early oral osseointegration: A comprehensive characterization in the Lewis rat

Sutton E. Wheelis
University of Texas at Dallas

Cláudia Cristina Biguetti
The University of Texas Rio Grande Valley, claudia.biguetti@utrgv.edu

Shruti Natarajan

Alexandra Arteaga
University of Texas at Dallas

Jihad El Allami
University of Texas at Dallas

See next page for additional authors

Recommended Citation

Wheelis, S. E., Biguetti, C. C., Natarajan, S., Arteaga, A., El Allami, J., Lakkasettar Chandrashekar, B., Garlet, G. P., & Rodrigues, D. C. (2021). Cellular and Molecular Dynamics during Early Oral Osseointegration: A Comprehensive Characterization in the Lewis Rat. ACS biomaterials science & engineering, 7(6), 2392–2407. https://doi.org/10.1021/acsbiomaterials.0c01420

HHS Public Access

Author manuscript

ACS Biomater Sci Eng. Author manuscript; available in PMC 2022 June 14.

Published in final edited form as:

ACS Biomater Sci Eng. 2021 June 14; 7(6): 2392–2407. doi:10.1021/acsbiomaterials.0c01420.

Cellular and molecular dynamics during early oral osseointegration: A comprehensive characterization in the Lewis rat

Sutton Elizabeth Wheelis[1], **Claudia C. Biguetti**[1], **Shruti Natarajan**[2,3], **Alexandra Arteaga**[1], **Jihad El Allami**[1], **Bhuvana Lakkasetter Chandrashekar**[1], **Gustavo Garlet**[4], **Danieli C. Rodrigues**[1,*]

[1]Deparment of Bioengineering, University of Texas at Dallas.

[2]Department of Biological Sciences, University of Texas at Dallas.

[3]Texas A&M College of Dentistry

[4]Bauru School of Dentistry, Department of Biological Sciences, University of São Paulo São Paulo, Brazil

Abstract

Objective: There is a need to improve the predictability of osseointegration in implant dentistry. Current literature uses a variety of *in vivo* titanium (Ti) implantation models to investigate failure modes, and test new materials and surfaces. However, these models produces a variety of results, making comparison across studies difficult. The purpose of this study is to validate an oral osseointegration in the Lewis rat to provide a reproducible baseline to track inflammatory response and healing of Ti implants.

Methods: Ti screws (0.76 mm Ø x 2 mm length) were implanted into the maxillary diastema of 52 adult male Lewis rats. Peri-implant tissues were evaluated 2, 7, 14, and 30 days after implantation (n = 13). Seven of the thirteen samples underwent microtomographic analysis, histology, histomorphometry and immunohistochemistry to track healing parameters. The remaining 6 samples underwent qPCR to evaluate gene expression of inflammation and bone remodeling markers over time.

[*]**Corresponding Author/Address: Dr. Danieli C. Rodrigues**, Danieli@utdallas.edu, 800 W Campbell Rd. BSB11, Richardson TX 75080.

Author Addresses:

Sutton Elizabeth Wheelis, 800 W Campbell Rd. BSB11, Richardson, TX 75080.

Claudia C. Biguetti, 800 W Campbell Rd., Richardson, TX 75080.

Shruti Natarajan, 800 W Campbell Rd., Richardson, TX 75080.

Alexandra Arteaga, 800 W Campbell Rd. BSB11, Richardson, TX 75080.

Bhuvana Lakkasetter Chandrashekar, 800 W Campbell Rd. BSB11, Richardson, TX 75080.

Jihad El Allami, 800 W Campbell Rd., Richardson, TX 75080.

Dr. Gustavo Garlet, Alameda Doutor Octávio Pinheiro Brisola, 9-75, Bauru - SP, Brazil, 17012-901.

Disclosures: The authors declare there are no conflicts of interest in this study.

Supporting Information

Histological graphic depicting the healing of sham surgeries at the osteotome site over time; histological graphic depicting the three failed implants from this study.

Results: This model achieved a 78.5 % success rate. Successful implants had 68.86% ± 3.15 BIC % at 30 days on average. Histologically, healing was similar to other rodent models: hematoma and acute inflammation at 2 days, initial bone formation at 7, advanced bone formation and remodeling at 14, and bone maturation at 30. qPCR indicated the highest expression of bone remodeling and inflammatory markers 2-7 days, before slowly declining to non-surgery control levels at 14-30 days.

Conclusion: This model combines cost-effectiveness and simplicity of a rodent model, while maximizing BIC, making it an excellent candidate for evaluation of new surfaces.

Graphical Abstract

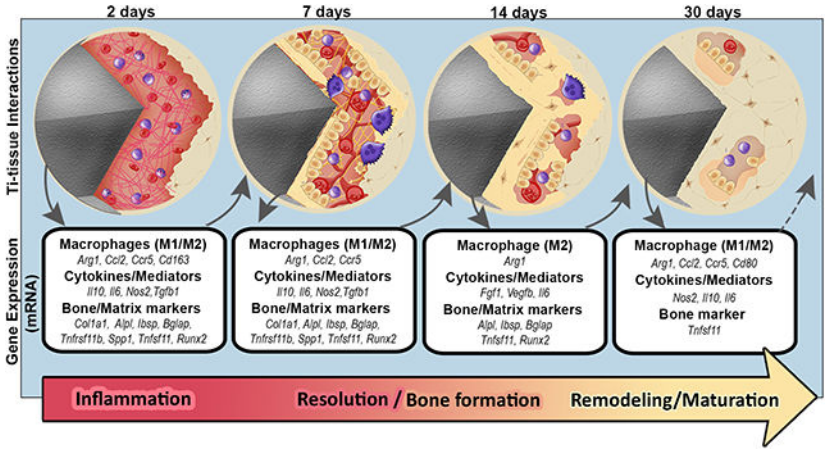

Keywords

Intramembranous Osseointegration; Rodent Model; Titanium

1. Introduction

Although titanium dental implants have been widely employed for the past 35 years, there is still a 'therapeutic window' and clinical necessity for bioengineering interventions aimed at increasing the predictability of achieving osseointegration in dentistry. Evaluating the probability that a particular implant will be successful is explored in the literature, but complete understanding of how this process occurs remains elusive as clinical data is highly heterogeneous. Moreover, successfully osseointegrated implants seldom undergo *ex vivo* analysis.[1-8] As a result, focus has been placed on the etiology of early dental implant failure (occurring in up to 4.6% implants placed), where osseointegration is never achieved.[9-12] These early failures can occur due to a variety of reasons, such as bacterial infiltration, surgical trauma, failure to achieve primary stability, and other patient factors like bone quality.[9-11,13-18] However, the underlying cause is a disruption in constructive titanium-tissue interactions that results in destructive inflammation and failure.[19-24] Our increased understanding that osseointegration is the result of a beneficial or constructive inflammatory process has led to the development and testing of new coatings and surface modifications on titanium implants. These surfaces are designed to mitigate external factors that interfere with constructive inflammation[25-30] while trying to encourage regenerative

healing in the early stages of implant placement via encouraging the M1-M2 macrophage polarization axis.[31,32,41,42,33-40]

In vitro models are often the initial tests performed with these new surfaces, where bone-forming, gingival, or immune cells are seeded on surfaces and evaluated for proliferation, differentiation, and various cytokine and growth factor expression.[43-52] These models are a good initial test to evaluate biocompatibility and are becoming more reflective of early healing scenarios, such as the "race-for-the-surface" by utilizing bacterial-mammalian cell co-culture models.[53-55] While useful to understand isolated variables, *in vitro* conditions cannot simulate the complex microenvironment resulting from dental implant placement. *In vivo* animal models overcome some of the limitations of *in vitro* models, providing a more clinically relevant environment to track healing. The literature contains a large variety of maxilla/mandible implantation models into larger animals such as sheep, dogs or mini pigs.[56-63] that more accurately simulate human occlusal loads, or rodent models that employ long bone implantation into the femur or tibia.[34,64-67] Large animal models could be considered ideal considering biomechanical approaches, but there are cost and ethical considerations when using these models. These are typically not cost effective, resulting in expensive housing and drug costs, keeping sample sizes low in addition to limited accessibility to commercial gene expression or enzyme-linked immunosorbent assays that allow for molecular events leading to osseointegration to be fully explored. Rodent long bone models are more cost-effective, however long bones undergo endochondral and intramembranous ossification in aseptic conditions. On the other hand, maxillofacial bones only undergo intramembranous ossification following injury.[68] As dental implants are placed in non-aseptic conditions with potential complicating factors such as pH, saliva flux, food bolus, and bacteria, the rodent oral cavity may be a more suitable region for preclinical research on oral osseointegration.

Oral osseointegration models in rodents provides the best of both worlds: they are more cost effective than large animal models and more reflective of the human oral environment and healing than long bone implantation. Fortunately, oral implantation models in rodents are not a novel concept. A number of studies have employed two particular types of maxilla implantation in the rodent: those which involve extraction of one or more of the first molars before placement of the implant (extraction models)[69,70,79-81,71-78] or direct implantation into the maxillary diastema without tooth extraction (non-extraction models).[82-87] Further examination of either of these models will uncover a large variety in methodology. In extraction models, the placement of the implant is reported to be either immediately following tooth extraction[69-71,73,80] or up to 30 days after.[72,74-79,81] Placement is also inconsistent, in bed of the first molar,[71,73-77,79,81] anywhere between the first and second molar,[70] or the socket where the mesial root of the first molar is located before extraction.[69,80] In non-extraction models, implantation into the maxillary diastema can occur anywhere anterior to the first molar and posterior of the incisor roots.[82,85,86] Finally, both models have a large variety of implant dimensions ranging from 0.67 mm – 1.7 mm in diameter and 2.0 mm- 4.5 mm in length.[73,76,82,84,88] One could argue that these variations in implantation procedures, implant size, and bone quality at different locations may reflect what happens in the clinic. However, these *in vivo* models strive to provide an accurate simulation of the best-case wound healing scenario and most neglect define success

criteria, success yield of their model, or links to human clinical osseointegration. Without a consistent methodology, it is difficult to evaluate the impact of a new implant surface/coating or material in the absence of a baseline or “ideal” osseointegration model.

Recently, Mouraret et al. developed a model and histological characterization of implantation into edentulous alveolar crest of the maxilla in CD1 mice.[89] This model was further supported by Biguetti et al., who provided a thorough histological, histomorphometric, microtomographic and molecular characterization of inflammatory, wound healing and bone remodeling events involved in early oral osseointegration of C57Bl/6 mice.[88] This study utilized a combination of techniques often singularly found in other rodent models to characterize early intramembranous osseointegration. This particular iteration of the non-extraction model resulted in a 77.78 % success rate and 81.03±3.87% new bone area within implant threads. These parameters make this model appealing for simulating human osseointegration, where 81.4% new bone area (BA) is observed and greater than 60% bone to implant contact (BIC) is considered successful for up to 17 years.[20,88,90] While promising, implantation space is limited in mice. Even in the most ideal cases, the width of the alveolar ridge is about 300 μm and the scale of implants used (0.67 mm diameter by 1.5 mm length) overwhelm the edentulous alveolar crest, protruding into the maxillary sinus, with new bone growing out and onto the implant in addition to replacing existing surrounding bone.[21,88,89]

Therefore, the aim of this study is to develop a new edentulous alveolar crest implantation model in the Lewis rat to provide an appropriate and reproducible baseline to track healing of titanium implants from initial injury to early osseointegration using molecular, histomorphometric, and microtomographic characterization. The use of this non-extraction model will provide decreased variation and potential complications proposed versus an extraction model, and rats are proposed to provide the advantages of increased scale (approximately 10X larger than mice), resulting in an alveolar ridge widths greater than 1 mm. Therefore, larger implants could be accommodated, eliminating implant fabrication issues, decreasing the surgical learning curve and providing larger amounts of supporting bone to increase BIC% and chance of primary stability. The combination of non-extraction model, ability for clinical translation, and breadth/depth of analysis at the cell and molecular is novel and unparalleled in the literature. It is hypothesized this model will achieve an osseointegration success rate similar to mice non-extraction models (>70%) with similar BIC and BA (84.9 % and 81.4 %, respectively) to those observed in humans, thus allowing it to be utilized to test new surfaces, coatings, and materials for dental implants.

2. Materials and Methods

2.1 Implants

Commercially pure titanium (cpTi) threaded dentin pins (0.76 mm ø x 2 mm, Fairfax Dental Inc., Miami, FL, USA) were used as implants in this study. All implants were cut to an approximate 2 mm length using orthodontic pliers and cleaned by sonicating for 45 min each in acetone, DI water, and ethanol solutions respectively. After sonication, implants were place in an oven at 65 °C to dry before being sterilized in an autoclave.

2.2 Animals

All animal surgeries, as well as pre- and post- operative care was carried out with supervision and approval from the Institutional Animal Care and Use Committee (IACUC #16-05) in compliance with the NIH Guide for the Care and Use of Laboratory Animals. This study was divided into 4 experimental groups of 13 adult male 10-12 week old Lewis Rats (Charles River Laboratories, Wilmington, MA, USA) ranging from approximately 250-325 grams in weight. The rats were maintained in the Vivarium at the University of Texas at Dallas with sterile water and dry food pellets available to animals *ad libitum*, except for 72 hours following surgery, in which the diet was crumbled and mixed with water. Experiment groups were separated by time points (2, 7, 14, and 30 days after implantation, n =13 per group) with an additional control group (n = 13) that received no surgery for a total of 65 animals.

2.3 Surgical Procedure

Rats were weighed before and after surgery to monitor body weight. The animals were anaesthetized by an intramuscular injection of 50-100 mg/kg ketamine hydrochloride and 20-50 mg/kg xylazine hydrochloride. After anesthesia, rats were placed in a dorsal decubitis position on a surgical table. Following positioning, animals were given an injection at the surgical site with 20 mg/kg of lidocaine with 1:100,000 epinephrine (Quala Dental Products, Nashville, TN, USA) for hemostasis and local analgesia. Implantation consisted of first making a 2 mm mucosal incision 1 mm in front of the right maxillary first molar to expose bone, followed by the drilling of a 0.67 mm implant bed using a surgical micromotor at 1000 RPM (NSK Surgic Pro) and subsequent placement of a 0.76 mm ø by 2 mm titanium screw in the edentulous alveolar crest osteotome site using needle holders (Figure 1). The left side of the maxilla was used exclusively for screw placement while the right side received just the incision and osteotome site (surgical sham) in the same rat. Additional control rats received no surgery (non-surgery controls). Feeding, drinking, and grooming were monitored daily during the post-operative period. At the end of the experimental periods (2,7,14 and 30 days), the animals were sacrificed with an overdose of pentobarbital sodium (Euthanasia III Med-Pharmex Inc., Pomona, CA, USA). After sacrifice, the implantation sites were cleaned briefly with saline before photos were taken using a stereomicroscope (Olympus, SMZ45T with DS-Fi2-L3 Camera, Shinjuku City, Tokyo, Japan) to track clinical healing of the oral mucosa covering the implant. Seven of the animals from each group had their whole maxilla placed in 10% neutral buffered formalin (NBF) for x-ray microtomography and histology. The remaining 6 had each tissue section containing an implants well as sham and control tissue excised from the animal with dissecting scissors and snap frozen for molecular analysis.

2.4 X-ray Microtomography (Micro-CT)

Micro-CT allowed evaluation of the position of the implant in relation to surrounding bone and osseointegration around implants. After fixation in NBF for 48 hours, samples were continuously washed in water for 24 hours to prevent over fixing, and finally placed in 70% ethanol until processing. Whole maxillae were assessed by Micro-CT (Skyscan 1272, Bruker, Billerica, MA, USA) at 100kv and 100 μA with 6.75 μm distance interval

for 180 degrees using a 0.4 degree step size and 0.11 mm copper filter. Projection files were reconstructed using NRecon Software (Bruker, Billerica, MA, USA), using a Gaussian smoothing kernel of 3, ring artefact correction of 6, and beam hardening correction of 40% to improve image reconstruction quality. Reconstruction files were evaluated using CT analyzer software (CTAn, Bruker, Billerica, MA, USA) to quantitatively determine mineralized bone around the implant. A constant region of interest 1 mm in diameter and 1.5 mm in length was defined along the medial portion of implant and surrounding bone, excluding 500 μm on the coronal portion of the implant where it emerged into oral cavity. Using these sagittal cross-sectional regions of interest saved from 2D CT images, percent of implant bone volume (BV) and tissue volume (TV) was determined to achieve the final parameter of BV/TV% to correlate to bone growth over time. 2D and 3D visualization of Micro-CT scans was achieved with Data Viewer and CTVox Software (Bruker, Billerica, MA, USA) respectively.

2.5 Histological Processing

After micro-CT processing, samples were decalcified in 11.2% ethylenediaminetetraacetic acid (EDTA)-2Na at 4°C for 2 weeks. After decalcification, whole maxillae were grossed down to transverse sections containing the implant. Following tissue processing with the implants in place, implants were carefully unscrewed from its coronal end before embedding in paraffin blocks. Twelve total 5 μm histological sections were made in the central region of titanium implant site per biological replicate. Six sets of 2 serial sections were made with 30 μm of separation to get a good representation of the sample for staining.

2.6 Histopathological and Histomorphometric Analysis

The progression of healing and osseointegration was evaluated using H&E and Masson's trichrome stain. One section at each depth (6 total) underwent a standard hematoxylin and eosin (H&E stain) for histopathological evaluation and histomorphometry. One section best representative of each time point was also stained using Masson's trichrome to track bone mineralization for qualitative analysis only. Evaluation of soft tissue integrity and mucosa–implant interface consisted of the area from alveolar bone crest to the point of implant emergence through oral epithelium of the peri-implant mucosa. Evaluation of hard tissue integrity consisted of the area of implant threads in contact/adjacent to alveolar bone, excluding any sample that penetrated the maxillary sinus. Soft tissue histomorphometry was used to quantify blood clot, blood vessels, inflammatory cells, foreign body giant cells (FBGC), fibroblasts, and fibers in three 173.4 μm x 130.1 μm histological fields per section at 400X magnification, which were averaged. Bone to implant contact percentage (BIC %) was calculated on 30 day samples using Cellsens software (Olympus, Shinjuku City, Tokyo, Japan) to measure the length of the alveolar bone in direct contact with the implant. Before measuring the length of the implant at the bone level, a horizontal line designating the crest of the maxillary bone and crest of maxillary sinus adjacent to the implant was drawn across the implant space of each section. Following this several measurements were taken:

1. The entire length of the implant under the crest of maxillary bone and above the crest of maxillary sinus (Implant Length).

2. The length of the implant in contact with bone under the crest of maxillary bone and above the maxillary sinus (Bone Contact).

BIC% was then calculated by using the equation: Equation 1.
Percentage of bone to implant contact.

$$BIC\,\% = \frac{Bone\ Contact}{Implant\ Length} * 100$$

Hard tissue histomorphometry was used to quantify blood clot, blood vessels, inflammatory cells, FBGC, fibroblasts, fibers, osteoblasts, osteoclasts, and new bone matrix in seven 173.4 μm x 130.1 μm histological fields per section at 400X magnification, which were averaged. 14 and 30 day samples with failed implants (absence of osseointegration) were excluded from analysis. The remaining 5 sections in each sample were used for immunohistochemistry.

2.7 Immunohistochemistry

Immunohistochemistry was used to identify and quantify osteoclasts and macrophages within threads adjacent to/in contact with alveolar bone. Osteoclasts were identified by Tartrate Resistant Acid Phosphatase (TRAP)[91] (anti-TRAP, 1:200 mouse monoclonal [ACP5/1070] (ab212723), Abcam, Cambridge, UK), and macrophages by using a universal macrophage marker (anti-CD68, 1:1000 Rabbit polycloncal (ab125212), Abcam, Cambridge, UK). Sections were first deparaffinized and underwent antigen retrieval by submersion in either Tris Buffer at pH 9.0 (CD68) or Citrate Buffer pH 6.0 (TRAP) maintained at 95 °C for 30 min. After washing in deionized (DI) water, the area of interest for staining was marked with a peroxidase-antiperoxidase (PAP) pen. Tissue was blocked with protein block provided from mouse and rabbit specific HRP/DAB (ABC) and Micropolymer Detection IHC Kit (Abcam, Cambridge, UK) and subsequently incubated with the selected primary antibody at 4 °C overnight in a humidified chamber. Two technical replicates from each sample were stained with each marker, in addition to a final sample that was incubated with 1% Bovine serum albumin in 1X phosphate buffered saline (Sigma-Aldrich, St. Louis, MO, USA) instead of a primary antibody as a negative control. After incubation, the slides were washed and blocked with hydrogen peroxide, before incubation with a biotinylated goat antipolyvalent secondary antibody and 3,3′-diaminobenzidine (DAB) chromagen, following the manufacturer's protocol from the HRP/DAB or Micropolymer Abcam IHC kit. Lastly, slides were counterstained in Mayer's Hematoxylin for 2 min and finished with Permount (Fisher Scientific, Hampton, NH, USA) and a coverslip. Seven 173.4 μm x 130.1 μm histological fields were captured comprising the region adjacent to the implant to quantify osteoclasts and macrophages. Three 173.4 μm x 130.1 μm histological fields were captured comprising the region from alveolar bone crest to the point of implant emergence through oral epithelium to quantify macrophages in the soft tissue. Cell counting was performed using the same technique employed with H&E stained sections. As CD68 is also a marker for PMN granulocytes such as neutrophils, these cells were identified based on their nuclear morphology and excluded from analysis so only macrophages were counted.

2.8 Molecular Analysis

Fresh tissue sections comprising the peri-implant mucosa and bone were snap frozen and stored at −80° C to preserve RNA integrity in order to perform gene expression analysis. Approximately 50 mg of peri-implant or control tissue from each sample were homogenized using the Bullet Blender Storm (Next Advance Inc., Troy, NY, USA) according to the protocol outlined by Carter et. al. 2012.[92] RNA was isolated using the RNeasy Mini-kit (Qiagen, Hilden Germany) following manufacturer's instructions. The concentration and quality of the RNA was verified with a spectrophotometer (NanoDrop™ 200, Fisher Scientific, Hampton, NH, USA) and a fragment analyzer (Agilent Technologies, Santa Clara, CA, USA). After isolation, cDNA synthesis was performed using qScript cDNA supermix (QuantaBio, Beverly, MA, USA), and cDNA reaction products were purified with the Qiaquick Purification Kit (Qiagen, Hilden Germany). qRT-PCR was performed with cDNA and TaqMan single tube assays (Applied Biosciences, Foster City, CA, USA) to quantify genes for macrophage polarization (*Arg1, Cd163, Nos2*), inflammation (*Ccr2, Ccr5, Cd80, Cxcl12, Il6, Il10*, and *Tnf*), tissue reconstruction and bone formation/remodeling (*Fgf1,Tgfb1, Vegfb*, *Col1a1, Alpl, Bmp2, Bmp7, Ibsp, Dmp1, Bglap* (produces Osteocalcin-OCN), Tnfrsf11b (produces Osteoprotegrin-OPG), *Spp1* (produces Osteopontin-OPN), *Tnfsf11* (produces RANKL), *Runx2,* and *Sost*) using 10 ng/μL of cDNA per reaction. Each sample reaction was performed in triplicate and contained a gDNA control to confirm that there was only template specific amplification. Data analysis was performed using the ΔΔCt method to compare each marker of interest with 3 housekeeping genes (*B2m, Hprt1, Ldha*), determining fold changes in uncoated Ti samples relative to a non-surgery control.

2.9 Statistical Analysis

Statistical analysis of BV/TV%, histomorphometry, and fold changes in gene expression from molecular analysis was performed using a one-way Analysis of Variance with a post hoc Tukey test to compare time points if samples demonstrated a normal distribution with a Shapiro-Wilk Normality test. If samples did not follow a normal distribution, the non-parametric Kruskal-Wallis test was performed with Dunn's multiple comparisons test. The Tukey/Dunn test made multiple comparisons to evaluate the significance between time point groups. Both tests were run in GraphPad Prism 7.0 software (GraphPad Software Inc., San Diego, CA, USA) using a significance level (α) of 0.05. P values were used to determine significance between groups.

3. Results

3.1 Clinical and Microtomographic Analysis

From a clinical perspective, rats exhibited no signs of hyperalgesia, with normal grooming, eating, and nesting behavior. Upon sacrifice and sample collection, macroscopic evaluation demonstrated no clinical signs of infection and all implants remained in place for the duration of the study. The initial healing of peri-implant mucosa and the sham (Figure 2) was observed at 2 days containing a film of fibrin over the surface of the implant. At 7 days there was oral epithelium and connective tissue growth with the absence of clinical inflammation (redness and swelling) in both uncoated implant and sham. At 14 and 30

days the oral mucosa was covering the implant completely and completely intact in the sham, with clinical health comparable to the controls. Residual blood observed between the maxillary molars of samples is an artifact from sample dissection at the time of sacrifice. Following microtomographic analysis of all samples, it was revealed that 12 of the 14 samples placed at 14 and 30 days achieved bone to implant contact, shown in Figure 3B. Reconstruction of microtomographic scans in 3D demonstrated an ingrowth of new bone into the threads at 7 days, visually increasing in volume within the threads at 14 and 30 days (Figure 3A). Morphometry data of μCT scans revealed a similar trend of an increase of BV/TV % from 7 and 14 to 30 days (Figure 3D).

3.2 Histopathological and Histomorphometric Analysis

Following histological evaluation, it was confirmed that of the 14 implants placed for 14 and 30 days, 11 were osseointegrated with 68.86 ± 3.51 BIC % at 30 days, resulting in a 78.5% success rate. The 3 implants with >40% fibrous encapsulation in the threads at the peri-implant bone level were designated as failures and were excluded from histomorphometric analysis. The samples that failed at 30 days were either close in proximity to the first molar root (Figure S2C), or contained sequestered fragments of bone (Figure S2A). The 14 day failure exhibited fibrous tissue populated with macrophages, active bone resorption and bone necrosis (Figure S2B). At 2 days, mononuclear cells, polymorphonuclear (PMN) cells and loose red blood cells (clot) were found among a fibrin matrix both adjacent to the supporting bone and peri-implant mucosa surrounding the implant space (Figure 4). Supporting bone close to the implantation site contained empty lacunae without osteocytes. At 7 days, implantation sites still exhibited the residual blood clot and inflammatory infiltrate, but there was evidence of loosely packed connective tissue at the mucosa level and bone remodeling at the supporting bone area. Bone remodeling was identified by areas around the threads that were a mix of connective tissue with mononuclear and fibroblast-like cells, multinucleated osteoclasts at the edge of the supporting bone (Figure 5D), and large amounts of osteoblasts (Figure 5A and 5B) interspersed at the cementing lines (or reversal lines) of supporting bones as well as in new primary bone forming within the threads. New primary bone apposition on supporting bone was identified by slightly basophilic cementing lines formed by active osteoblasts (cells presenting a robust cytoplasm and cuboidal shape) on supporting bone and new osteoid (non-mineralized bone matrix) containing multiple new embedded osteocytes. Osteoid was evidenced by blue staining and the supporting bone by red staining in trichrome stain (Figure 4, 5A and 5B). At 14 days, some of the residual supporting bone with empty lacunae was in contact by newly formed bone, suggesting that the residual fragments of old bone were incorporated by the newly formed bone, serving as a bone graft. H&E staining revealed a more advanced stage of bone apposition, containing vessels surrounding implant threads spaces with fewer mononuclear cells fibroblast-like cells, and osteoclasts. In addition, this advanced stage of bone remodeling and maturation was also indicated by basic bone remodeling units (Figure 5). Osteoblast-shaped cells were still present as bone lining cells, although new bone appeared to have more mature osteocytes within lacunae, along with small islands of red stained mineralized bone in the trichrome stain. At the peri-implant mucosa level, there was vessel formation and more densely packed connective tissue populated with fibroblast and mononuclear cells. At 30 days, bone was dominated by more mature bone matrix, containing osteocytes and vessels

that appeared to be mineralized due to the matrix's red appearance in the trichrome stain, with a few osteoblasts adjacent to threads. Inflammatory infiltrate was negligible at both the peri-implant bone and mucosa levels. Densely packed connective tissue containing fibroblasts and vessels were located at the peri-implant mucosa.

Sham tissue containing just the osteotome site demonstrated similar healing benchmarks as the uncoated Ti (Figure S1). At 2 days, the osteotome site at the mucosal and bone level was filled with blood clot, MN and PMN cells within a fibrin matrix just as the implant thread spaces were in uncoated Ti samples. At 7 and 14 days there was evidence of new connective tissue, vessels. Inflammatory infiltrate, and fibroblasts at the mucosal level and new bone formation and remodeling at the bone level. New bone was formed in a large amount of areas at 7 days within the osteotome site with the space in between occupied by new vessels, osteoblasts, osteoclasts, monocytes, and fibroblast-like cells. At 14 days, vessels, fibroblasts and new connective dominated at the mucosal level, and there was more continuous new bone area at the osteotome site adjacent to the supporting bone, with the same structures and cell types occupying the non-bone space as the 7 day time point. At the 30 day time point, soft tissue at the mucosal level appeared dense, populated with vessels and fibroblasts with negligible inflammatory infiltrate. At the bone level, bone appeared continuous and mature with lacunae filled with osteocytes and new vessels, similar to control maxillary bone.

Histomorphometry of soft and hard peri-implant tissues supports histopathological observations at each time point, in addition to providing quantitative evidence of temporal cell behavior. At 2 days, the soft tissue contained a high density of blood clot, fibers and inflammatory cells compared to the other histomorphometry elements. At 14 and 30 days, there was a significant decrease in blood clot density ($p < 0.01$). Inflammatory cells demonstrated a similar trend as blood clot, significantly decreasing from 2 and 7 days compared to 14 and 30 day density ($p < 0.05$). However, unlike the blood clot density, soft tissue fibers demonstrated an increasing trend over all four time points, with statistically significant increases from 2 to 7 days, 14 to 30 days, and 2 to 30 days ($p < 0.05$). Fibroblasts and vessels followed the same positive trend as fibers, significantly increasing from 2 to 14 days ($p < 0.01$). Finally, soft tissue foreign-body giant cells (FBGC) were present in some samples resulting in a low density at 7 days and 14 days, but were absent at 2 and 30 days.

Hard tissue histomorphometry exhibited some of the same temporal patterns observed in the soft tissue. At 2 days, bone exhibited a large area density of blood clot content and inflammatory cells. Blood clot levels significantly decreased at 14 and 30 days from the 2 day time point ($p < 0.01$), while inflammatory cells had an increasing trend from 2 to 7 days, before significantly decreasing at 14 and 30 days ($p < 0.01$). Like soft tissue, FBGC were sporadically present in only a few histological sections from 4 samples. At the 7 day point, the presence of fibers and fibroblasts peaked in density at 7 and 14 days before significantly decreasing at the 30 day time point, unlike soft tissue ($p < 0.05$). Vessels exhibited the same trend as fibroblasts from 2 to 14 days, but remained similar in density to their 14 day peak at 30 days. Finally, results from osteoblasts, osteoclasts, and new bone matrix density exhibited bone remodeling dynamics. At 2 days, neither osteoclasts nor osteoblasts were present, while both cell types had a significant increase at 7 days. Proportionally, the density of osteoblasts was more than twice compared to osteoclasts ($p < 0.05$). At 14 days, presence

of osteoblasts continued to be very dense, along with the increase in new bone matrix from 2, 7, 14, and 30 days. On the other hand, osteoclasts showed a decreasing trend before significantly decreasing to a similar density seen at the 2 day time point at 30 days ($p < 0.01$). Osteoblasts density also presented a decreasing trend at 30 days, but still were higher in density than osteoclasts at their peak activity.

3.3 Immunohistochemistry for Macrophages and Osteoclasts

Immunohistochemistry was used to qualitatively (Figure 7B-C) and quantitatively (Figure 7A) evaluate two monocytes lineage cells involved in the osseointegration process, TRAP + osteoclasts and CD68+ macrophages. TRAP+ cells were overall low in density. These cells were barely observed at 2 days, but increased significantly at 7 and 14 days, before demonstrating a decreasing trend at 30 days. The density, morphology and location of TRAP+ cells were consistent with osteoclasts observed in H&E stains, being multinucleated and having their apical domain visible on the surface of peri-implant bone (Figure 7B). CD68+ cells in soft tissue demonstrated a more static presence histomorphometrically, while qualitative observations indicated an overall visual decrease in density from 2 to 30 days, with a few exceptions at 14 and 30 days, which demonstrated a visual density similar to the 2 day level. CD68+ cells in hard tissue indicated an overall decreasing trend from 2 to 30 days visually and histomorphometrically. The morphology of CD68+ cells were consistent with macrophages, while the location and density was similar in both hard and soft tissue (Figure 7C).

3.4 Molecular Analysis

RT-qPCR was performed on peri-implant tissue in order to quantify temporal changes in gene expression of 25 markers associated with osseointegration following implant placement, shown as mean fold change in expression relative to the non-surgery control (Figure 8A); and with individual samples graphed with 95% CI (Figure 8B). Markers associated with the inflammatory response (*Arg1, Ccl2, Ccr5, Cd163, Il10, Il6, Nos2*) experienced the highest mean up-regulation at 2 days post implantation from the non-surgery control. Pro-inflammatory markers *Cd80* and *Tnf* were upregulated at 2 days but not to the same magnitude as other inflammatory markers. Within this inflammatory marker group there are a few expression trends. *Arg1, Ccl2, Il6,* and *Nos2* were significant down-regulated over time. *Arg1* decreased significantly from 2 to 7, 14, and 30 days, although consistently up-regulated at all times compared to the control. *Ccl2*, *Cd163, Il6,* and *Nos2* significantly down regulated from to 2 to 14 days, while at 30 days there was an up-regulation trend from 14 days for all these markers. *Ccr5, Cd80* and *Tnf* experienced this same trend: a down-regulation from 2 to 14 days followed by an up-regulation from 14 to 30 days. *Cxcl12* maintained levels similar to the control at all time points.

The tissue reconstruction and bone remodeling markers also demonstrated a few expression trends. Of this group *Col1a1, Fgf1, Tgfb, Alpl, Ibsp, Bglap, Spp1*, and *Runx2* had the highest mean upregulation compared to the control at 2 days. *Spp1* maintained a similar level of expression at 7 days before significantly decreasing from 2 to 30 days. *Col1a1, Tgfb1, Alpl, Ibsp Bglap*, and *Runx2* maintained a similar but non-significant trend to *Spp1*, decreasing steadily in expression from 2 to 30 days. However, *Fgf1* expression was only

similar to its 2 day expression at 14 days, with 7 and 30 day expression being similar to the control. *Vegfb, Bmp2, Bmp7, Dmp1, Tnfrsf11b, Tnfsf11*, and *Sost* were all up-regulated in expression compared to the control at 2 days, although less in magnitude than the previous group. *Vegfb, Bmp2, Bmp7, and Dmp1* had their highest expression at 2 and 14 days, while at 7 and 30 days they decreased to the control level. Finally *Tnfrsf11b* expression peaked at 2 days, subsequently decreasing in expression from 2 to 14 days, before reaching control levels at 30 days, in contrast to *Tnfsf11*, which expressed steadily from 2 to 14 days before peaking at 30 days. Examining the individual dispersion graph there are several trends that correspond to heat map data, with one or two data points from each samples being outside the 95 % confidence interval demonstrating variation in expression from animal to animal, which did not affect the overall observed trends.

4. Discussion

There is a recent consensus in the literature that improved tools are needed to elucidate the mechanisms behind human osseointegration.[1,3] Existing *in vitro* and *in vivo* models of titanium implantation lack consistency in methodology, making reproducibility and comparisons between studies difficult. The aim of this study is to develop an oral osseointegration model in the Lewis rat to characterize the healing response of titanium implants from initial injury to early osseointegration at cellular and molecular levels. By utilizing molecular, histomorphometric, and microtomographic characterization, this model has the potential to not only allow a more comprehensive grasp of osseointegration, but provide a template for evaluation of new materials and surface coatings.

Clinical understanding of osseointegration in implant dentistry has most often been defined using macroscopic and radiographic methods.[3] Macroscopic evaluation of this model shows suitable peri-implant mucosa healing progression (Figure 2) and comparable 78.5% osseointegrative success versus the 77.78% and 74.1% compared to already established mice models.[88,89] The increased scale of rats provides an additional advantage of providing up to 1 mm length of bone to implant contact with 65.91 ± 10.7 % BV/TV at 30 days (Figures 3, 5, and 6), versus the 300 μm and 42.12 ± 3.01% BV/TV at 21 days achieved in a similar mice model.[88] This model also confirms the hypothesis that similar BA (73.94% ± 2.684, Figure 6) can be observed to what is seen in humans (81.8%).[93] In addition, this model provided the advantage of being more anatomically favorable than mice to accommodate larger implants, with more of the implant surrounded by supporting bone (Figure 5), versus existing mice models, where the implant protrudes out through the maxillary sinus.[88,89] This model has also demonstrated that it is able to achieve similar BIC%, BA, and BV at 4 weeks post-implantation as rat extraction models, while saving time and potential inflammatory variation or post-surgical complications (i.e. root fractures) following tooth extraction.[69,70]

Histological and molecular data allows a more detailed evaluation of intramembranous osseointegration from initial placement to primary bone contact. Tracking the dynamics of molecular response along with cellular changes is crucial to understand the mechanisms governing osseointegration. Immediately following implant placement, the peri-implant cavity is flooded with blood from the osteotome site, shown in Figure 5. The interaction between blood proteins adsorbed onto the surface of the Ti implant with leukocytes,

platelets, and damage-associated molecular patterns (DAMPs) produced from the surgical trauma trigger the innate immune response.[21,88] This pro-inflammatory cascade forms a blood clot in the peri-implant space, containing a provisional matrix of fibrin containing platelets, polymorphonuclear (PMN), mononuclear (MN), and red blood cells.[94] In our results, blood clot is observed at 2 days following implantation histologically in Figure 5, showing a loose fibrin matrix within the implant thread space adjacent to supporting bone. Histopathological analysis using H&E confirms the presence of these PMNs, red blood cells, and mononuclear cells within both soft and hard tissue, with similar histological observations seen in other rodent models.[69,74,76,88] A population of CD68+ macrophages are also observed at their highest density in both soft and hard tissue (Figure 4, 6, and 7). Gene expression (Figure 8) also supports the presence of this pro-inflammatory response through the up-regulation of monocyte/macrophage chemoattractant *Ccl2* and *Ccr5.*[50,95] The recruitment of these cells, especially macrophages, are directly involved in the next stages of bone remodeling necessary for osseointegration. At this time point, markers for pro-inflammatory macrophages (*Cd80, Nos2, Tnf*) were significantly increased in sites of implantation. It has been demonstrated that IL6, NOS2, and TNF *are* expressed by inflammatory cells, which encourage M1 macrophage polarization were also up-regulated.[88,96-99] While a pro-inflammatory environment is essential to begin the wound healing progress, the polarization of macrophages from the M1 to M2 phenotype is essential for the resolution of inflammatory process and to a constructive healing.[23] Interestingly, at 2 days, M2 markers (*Il10, Arg1* and *Cd163*) were also upregulated as well.[99] ARG1 is produced upon PMN cell death, making it a regulator of the innate immune response, and is also associated with M2 macrophage polarization, which express CD163.[32,98,100] Additonally, IL10 has been demonstrated as a cytokine involved in the resolution of inflammation produced by macrophages.[99] The expression profile of these inflammatory markers at 2 days is very similar to what is seen in other literature involving humans, rats, and mice.[4,5,7,80,88,101]

At this point it is important to consider the histological and histomorphometric healing progression from 2 to 7 days in Figure 4 and 6. While at 2 days, the peri-implant space is largely dominated by blood clot, at 7 days there is a significant increase in osteoclasts, osteoblasts and new bone matrix along with an increasing trend for vessels and fibroblasts. This suggests that the bone remodeling process is being initiated sometime before 7 days post implantation, which was also observed to occur at this time point in other rat models.[69,74,76] Additionally, histomorphometry (Figure 6) indicates the average area density of osteoclasts (1.162 %), osteoblasts (3.248%), and bone matrix (16.58 %) at 7 days in this model is higher than in a similar implantation model in mice (approximately 0 %, 2%, and 7% for osteoclasts, osteoblasts and bone matrix, respectively).[88] This histological data suggests the start of bone remodeling may be occurring at earlier stages than similar non-extraction mice models.[88,89] The balance of supporting bone resorption and new bone deposition is controlled via inflammatory cells and their markers. These cells and proteins encourage osteoclastogenesis (resorption) and differentiation of osteoblasts (deposition) and endothelial cells from mesenchymal stems cells (MSCs).[94,102] The cascade of events that result in bone resorption begin at the site of injury. Apoptotic osteocytes from damaged supporting bone release RANKL,[68] whose expression is also upregulated by other members

of the NF-κβ signaling family, IL6 and TNF.[103] RANKL is the key protein associated with macrophage fusion and differentiation into osteoclasts.[103,104] Again, *Il6, Tnf* and *Tnfsf11* are all upregulated 2 and 7 days in this model (Figure 8), indicating that osteoclastogenesis may be occurring at these time points, as confirmed by histological, histomorphometric, and IHC (TRAP+) data that supports this gene expression profile, as osteoclasts are most area dense at the 7 day time point. Similarly, the cascade of events that result in osteoblast differentiation begin following injury. Platelets located within the peri-implant blood clot release VEGFB and TGFB1 [105]. VEGF is key in regulating neovascularization via activation of endothelial cells, in addition to proposed chemoattractant activity for MSCs.[106,107] In accordance with histomorphometric results, there is a significant increase in vessels and hard tissue fibroblasts (indistinguishable from MSCs) density from 2 to 14 days in Figure 6 along with high *Vegfb* expression at 2 and 14 days in Figure 8. TGFB1, although also associated with angiogenesis, is mostly known for MSC recruitment and belongs to the same TGFB protein superfamily as BMP2 and BMP7.[108] Collectively, TGFB1, BMP2, BMP7 have an osteogenic effect via differentiation of MSCs to the osteoblast phenotype.[108,109] In existing rodent models, MSC recruitment and angiogenic markers are often expressed at their highest at the 7 and 14 day time points, while in this model, these angiogenic and MSC recruitment markers (*Tgfb1, Bmp2,* and *Bmp7*) are expressed at their highest at the 2 day time point.[76,80,88] This is again supporting evidence that bone remodeling may be occurring at a faster rate in this model than in other rodent models.

BMP signaling results in the activation of *Runx2*, the key transcription factor that encourages the MSC to differentiate to the osteoblast phenotype.[110] Following differentiation, osteoblasts secrete a variety of proteins that constitute the non-mineralized bone matrix.[68] Histologically, osteoblasts, osteoclasts are actively remodeling the new bone matrix at 7 and 14 days, even forming bone matrix units (BMU) containing an osteoblast, osteoclast and vessel (Figure 5). This is supported by the upregulation of *Col1a1, Alpl, Runx2, Ibsp, Tnfrsf11b, Bglap*, and *Spp1* while *Tnfsf11* remains upregulated. COL1A1, ALP and OPN in particular are early osteogenesis matrix proteins secreted by osteoblasts while BSP, OCN, and DMP1 are more mature osteoblast markers involved in mineralization.[88,111-117] OPG is also notable as an decoy receptor for RANKL, inhibiting osteoclast activity and maintaining the delicate balance of bone resorption/deposition associated with successful osseointegration.[104] At this point it's important to consider that there is a pattern of expression wherein most bone of these remodeling markers are up-regulated the highest at 2 days before demonstrating a decreasing trend over time (Figure 8), whereas other literature in mice, rats, and humans suggests these markers peak in expression 7-14 days post implantation.[1,4-6,8,73,76,80] There are several potential reasons for this contrast in expression. First, it is difficult to make direct comparisons across models due to variations in time point (1-4 days at first collection), the source of the mRNA (fresh or FFPE peri-implant tissue, the implant surface, or peri-implant sulcus fluid, and sample size.[1,4-8,66,80,88,101] Second, the main aims of these studies is often to evaluate changes between implant surfaces and patient factors, not to understand the temporal behavior of these genes.[6-8,66] All of these elements can effect gene expression data. It is hypothesized that in this particular model, markers express the highest around the 2 day time point, because all the transcription factors/proteins necessary for osteoclast/

osteoblast differentiation need to be translated before all the remodeling activity starting at 7 days. There is some support from human gene expression profiles that bone remodeling markers like, *IBSP, SPP1, RUNX2, BGLAP, COL1A1* are upregulated as early 1-3 days post-implantation.[1,8,101] From 7 to 14 days, there is similar rate of bone remodeling observed from 2 to 7 days. This is supported by continued mRNA expression at 7 days of *Ibsp, Alpl, Bglap, Tnfrsf11b, Tnfsf11, Runx2, and Spp1*. As the rate of bone formation, osteoblast and osteoclast cell density decreases from 14 to 30 days, these same markers show a stagnating or decreasing trend in their expression to reflect this. Finally, osteocyte marker *Sost* and mineralization marker *Dmp1* is upregulated at 2 days, but this appears to be one sample outside upper limit of the 95% CI of the 2 day time point, therefore the 2 day mean does not necessarily indicate mineralization or osteocyte expression at 2 days.

At 30 days there is several interesting trends when comparing gene expression to histological and microtomographic data. Using histological and microtomographic methods it's evident that successful osseointegration and mineralization is present from 14 to 30 days in Figure 3 and 6. There is an increasing trend in BV/TV% from 7 to 30 days, a significant upregulation of bone area density to 73.96 ± 2.684 %, and mineralization of this new bone indicated in the trichrome stain. This mineralization behavior is consistent with the trichrome stain in similar rat implantation models.[69,118] The resolution of inflammation and healing process is also supported by a decreasing trend in general inflammatory cells, and CD68+ macrophages. Simultaneously, all pro-inflammatory markers *Ccr5, Ccl2, Cd80, Nos2, Il6*, and *Tnf* are downregulated from 2 to 14 days in accordance with histological observations, as well as supported by other rodent and human expression profiles.[4,7,8,88,101]

Interestingly, there is an upregulation of these pro-inflammatory markers in addition *Tnfsf11* at the 30 day time point. In experimental animal models, successful osseointegration is defined by histopathological observations more than clinical or radiographic analysis. This model has a 78.5 % success rate derived from histological data due to the fact failures can be easily identified and excluded by the inspection of H&E histological sections. The 21.5% of implants that failed histologically were either partially (>40%, Figure S2A) or fully encapsulated with fibrotic tissue (Figure S2B-C), with potential causes being implant instability (micro-motion) due to their proximity to the first molar root, or possible infection due to accumulation of neutrophils and FBGC around a sequestered bone fragment (Figure S2A). However there is no consensus on how to identify failures based on gene expression data alone. Evidence from our success rate indicates up to 12.5 % or 5 of 24 the samples that underwent gene expression analysis are failures. The literature suggests that successfully osseointegrated implants would demonstrate a gene expression profile similar to the 14 day samples: upregulation of anti-inflammatory, bone matrix, and, osteoclastogenic inhibiting *Tnfrsf11b* indicating healing is complete.[1,5,21,88] Pro-inflammatory genes *Nos2, Crr5, Ccl2, Cd80*, are all associated with the upregulation of *Tnfsf11*, osteoclastogenesis, and bone resorption. If the upregulation of these markers is prolonged and predominant at later healing time points (14 and 30 days), they could be associated with implant failures. Therefore it is possible that several samples within the 30 day time points for gene expression have failed, and that is skewing the mean expression profile towards chronic inflammation and resorption, although more literature on gene expression of failed implants is needed to support this claim.

The fact that comparisons between histological and gene expression comparisons are constrained by our understanding of the mRNA profile of implant failures is a limitation of this study. Microtomographic methods also have some limitations. While it is easy to identify whether or not an implant is osseointegrated with this method, 3D morphometry of bone volume seems to work optimally when a larger ROI is observed, such as a rodent tibia, or the aim is to compare osseointegration of implants in animals with varied bone quality.[82,88] Additionally, although inflammatory marker expression is very similar to humans, rats appear to progress through bone remodeling benchmarks faster than humans.[119] However, the overall process of intramembranous osseointegration remains similar to human studies, in addition to confirming the hypothesis that we can achieve > 70% success with similar bone area in human bone models with the combined advantages of a simpler surgical design and more tissue to implant contact.

5. Conclusion

This study elucidated the dynamics of cellular and molecular events involved in early oral osseointegration in a novel Lewis rat model. Taking into consideration all metrics, maxillary implantation into the edentulous alveolar crest with the appropriate length implant combines the cost-effectiveness of a rodent model, simplicity of a non-extraction model, and maximizes bone to implant contact. Due to the depth of analysis, high success rate and similarity to human osseointegration, this Lewis rat model is an excellent candidate for further evaluation of new materials and surfaces in the field of implant dentistry.

Supplementary Material

Refer to Web version on PubMed Central for supplementary material.

Acknowledgements:

The authors would like to thank John M. Shelton, Cameron Perry, and Maria Fernanda Felipa-Lastarria from the University of Texas Southwestern Medical Center Histo Pathology core for their guidance, expertise, collaboration and services. In addition, we would like the thank Dr. Anthony Melchiorri and Sean Bittner of Rice University for their assistance and access to their Bruker Skyscan 1272. Finally, we would like to thank Dr. Yeun Hee Kim from the UT Dallas Genome Core for allowing us to use their equipment for qPCR analysis.

Funding:

This study was supported by a grant by the National Institute of Dental and Craniofacial Research (NIDCR/NIH) (Project #1R01DE026736).

References

(1). Bielemann AM; Marcello-Machado RM; Del Bel Cury AA; Faot F Systematic Review of Wound Healing Biomarkers in Peri-Implant Crevicular Fluid during Osseointegration. Arch. Oral Biol 2018, 89 (February), 107–128. 10.1016/j.archoralbio.2018.02.013. [PubMed: 29510331]

(2). Bencharit S; Morelli T; Barros S; Seagroves JT; Kim S; Yu N; Byrd K; Brenes C; Offenbacher S Comparing Initial Wound Healing and Osteogenesis of Porous Tantalum Trabecular Metal and Titanium Alloy Materials. J. Oral Implantol 2019, 45 (3), 173–180. 10.1563/aaid-joi-D-17-00258. [PubMed: 30663941]

(3). Shah FA; Thomsen P; Palmquist A Osseointegration and Current Interpretations of the Bone-Implant Interface. Acta Biomater. 2019, 84, 1–15. 10.1016/j.actbio.2018.11.018. [PubMed: 30445157]

(4). Thalji GN; Nares S; Cooper LF Early Molecular Assessment of Osseointegration in Humans. Clin. Oral Implants Res 2014, 25 (11), 1273–1285. 10.1111/clr.12266. [PubMed: 24118318]

(5). Sayardoust S; Omar O; Norderyd O; Thomsen P Clinical, Radiological, and Gene Expression Analyses in Smokers and Non-Smokers, Part 2: RCT on the Late Healing Phase of Osseointegration. Clin. Implant Dent. Relat. Res 2017, 19 (5), 901–915. 10.1111/cid.12514. [PubMed: 28744993]

(6). Sayardoust S; Omar O; Thomsen P Gene Expression in Peri-Implant Crevicular Fluid of Smokers and Nonsmokers. 1. The Early Phase of Osseointegration. Clin. Implant Dent. Relat. Res 2017, 19 (4), 681–693. 10.1111/cid.12486. [PubMed: 28470893]

(7). Sayardoust S; Omar O; Norderyd O; Thomsen P Implant-Associated Gene Expression in the Jaw Bone of Smokers and Nonsmokers: A Human Study Using Quantitative QPCR. Clin. Oral Implants Res 2018, 29 (9), 937–953. 10.1111/clr.13351. [PubMed: 30168218]

(8). Bryington M; Mendonça G; Nares S; Cooper LF Osteoblastic and Cytokine Gene Expression of Implant-Adherent Cells in Humans. Clin. Oral Implants Res 2014, 25 (1), 52–58. 10.1111/clr.12054. [PubMed: 23057568]

(9). Malm MO; Jemt T; Stenport V Early Implant Failures in Edentulous Patients: A Multivariable Regression Analysis of 4615 Consecutively Treated Jaws. A Retrospective Study. J. Prosthodont 2018, 27 (9), 803–812. 10.1111/jopr.12985. [PubMed: 30307086]

(10). Manzano G; Montero J; Martín-Vallejo J; Del Fabbro M; Bravo M; Testori T Risk Factors in Early Implant Failure: A Meta-Analysis. Implant Dent. 2016, 25 (2), 272–280. 10.1097/ID.0000000000000386. [PubMed: 26836129]

(11). Grisar K; Sinha D; Schoenaers J; Dormaar T; Politis C Retrospective Analysis of Dental Implants Placed Between 2012 and 2014: Indications, Risk Factors, and Early Survival. Int. J. Oral Maxillofac. Implants 2017, 32 (3), 649–654. 10.11607/jomi.5332. [PubMed: 28212455]

(12). Esposito M; Thomsen P; Ericson LE; Lekholm U Histopathologic Observations on Early Oral Implant Failures. Int. J. Oral Maxillofac. Implants 2000, 14 (6), 798–810.

(13). Olmedo-Gaya MV; Manzano-Moreno FJ; Cañaveral-Cavero E; De Dios Luna-Del Castillo J; Vallecillo-Capilla M Risk Factors Associated with Early Implant Failure: A 5-Year Retrospective Clinical Study. J. Prosthet. Dent 2016, 115 (2), 150–155. 10.1016/j.prosdent.2015.07.020. [PubMed: 26545864]

(14). Ducommun J; El Kholy K; Rahman L; Schimmel M; Chappuis V; Buser D Analysis of Trends in Implant Therapy at a Surgical Specialty Clinic: Patient Pool, Indications, Surgical Procedures, and Rate of Early Failures—A 15-Year Retrospective Analysis. Clin. Oral Implants Res 2019, 30 (11), 1097–1106. 10.1111/clr.13523. [PubMed: 31400242]

(15). Chrcanovic BR; Kisch J; Albrektsson T; Wennerberg A Factors Influencing Early Dental Implant Failures. J. Dent. Res 2016, 95 (9), 995–1002. 10.1177/0022034516646098. [PubMed: 27146701]

(16). Sakka S; Baroudi K; Nassani MZ Factors Associated with Early and Late Failure of Dental Implants. J. Investig. Clin. Dent 2012, 3 (4), 258–261. 10.1111/j.2041-1626.2012.00162.x.

(17). Santos MCLG; Campos MIG; Line SRP Early Dental Implant Failure : A Review of the Literature. Brazilian J. Oral Sci 2002, 1 (3), 103–111. 10.20396/bjos.v1i3.8641045.

(18). Sridhar S; Wang F; Wilson TG; Valderrama P; Palmer K; Rodrigues DC Multifaceted Roles of Environmental Factors toward Dental Implant Performance: Observations from Clinical Retrievals and in Vitro Testing. Dent. Mater 2018, 34 (11), e265–e279. 10.1016/j.dental.2018.08.299. [PubMed: 30220507]

(19). Trindade R; Albrektsson T; Tengvall P; Wennerberg A Foreign Body Reaction to Biomaterials: On Mechanisms for Buildup and Breakdown of Osseointegration. Clin. Implant Dent. Relat. Res 2016, 18 (1), 192–203. 10.1111/cid.12274. [PubMed: 25257971]

(20). Trindade R; Albrektsson T; Wennerberg A Current Concepts for the Biological Basis of Dental Implants: Foreign Body Equilibrium and Osseointegration Dynamics. Oral Maxillofac. Surg. Clin. North Am 2015, 27 (2), 175–183. 10.1016/j.coms.2015.01.004. [PubMed: 25753575]

(21). Biguetti CC; Cavalla F; Silveira EV; Tabanez AP; Francisconi CF; Taga R; Campanelli AP; Trombone APF; Rodrigues DC; Garlet GP HGMB1 and RAGE as Essential Components of Ti Osseointegration Process in Mice. Front. Immunol 2019, 10. 10.3389/fimmu.2019.00709.

(22). Sheikh Z; Brooks PJ; Barzilay O; Fine N; Glogauer M Macrophages, Foreign Body Giant Cells and Their Response to Implantable Biomaterials. Materials (Basel). 2015, 8 (9), 5671–5701. 10.3390/ma8095269. [PubMed: 28793529]

(23). Miron RJ; Bosshardt DD OsteoMacs: Key Players around Bone Biomaterials. Biomaterials 2016, 82, 1–19. 10.1016/j.biomaterials.2015.12.017. [PubMed: 26735169]

(24). Miron RJ; Zohdi H; Fujioka-Kobayashi M; Bosshardt DD Giant Cells around Bone Biomaterials: Osteoclasts or Multi-Nucleated Giant Cells? Acta Biomater. 2016, 46, 15–28. 10.1016/j.actbio.2016.09.029. [PubMed: 27667014]

(25). Vargas-Reus MA; Memarzadeh K; Huang J; Ren GG; Allaker RP Antimicrobial Activity of Nanoparticulate Metal Oxides against Peri-Implantitis Pathogens. Int. J. Antimicrob. Agents 2012, 40 (2), 135–139. 10.1016/j.ijantimicag.2012.04.012. [PubMed: 22727529]

(26). Kazemzadeh-Narbat M; Noordin S; Masri BA; Garbuz DS; Duncan CP; Hancock REW; Wang R Drug Release and Bone Growth Studies of Antimicrobial Peptide-Loaded Calcium Phosphate Coating on Titanium. J. Biomed. Mater. Res. B. Appl. Biomater 2012, 100 (5), 1344–1352. 10.1002/jbm.b.32701. [PubMed: 22566395]

(27). Liu R; Tang Y; Zeng L; Zhao Y; Ma Z; Sun Z; Xiang L; Ren L; Yang K In Vitro and in Vivo Studies of Anti-Bacterial Copper-Bearing Titanium Alloy for Dental Application. Dent. Mater 2018, 34 (8), 1112–1126. 10.1016/j.dental.2018.04.007. [PubMed: 29709241]

(28). Yuran S; Dolid A; Reches M Resisting Bacteria and Attracting Cells: Spontaneous Formation of a Bifunctional Peptide-Based Coating by On-Surface Assembly Approach. ACS Biomater. Sci. Eng 2018, 4, 4051–4061. 10.1021/acsbiomaterials.8b00885. [PubMed: 33418805]

(29). Tîlmaciu CM; Mathieu M; Lavigne JP; Toupet K; Guerrero G; Ponche A; Amalric J; Noël D; Mutin PH In Vitro and in Vivo Characterization of Antibacterial Activity and Biocompatibility: A Study on Silver-Containing Phosphonate Monolayers on Titanium. Acta Biomater. 2015, 15, 266–277. 10.1016/j.actbio.2014.12.020. [PubMed: 25562573]

(30). Xie K; Zhou Z; Guo Y; Wang L; Li G; Zhao S; Liu X; Li J; Jiang W; Wu S; Hao Y Long-Term Prevention of Bacterial Infection and Enhanced Osteoinductivity of a Hybrid Coating with Selective Silver Toxicity. Adv. Healthc. Mater 2019, 8 (5), 1801465. 10.1002/adhm.201801465.

(31). Brown BN; Ratner BD; Goodman SB; Amar S; Badylak SF Macrophage Polarization: An Opportunity for Improved Outcomes in Biomaterials and Regenerative Medicine. Biomaterials 2012, 33 (15), 3792–3802. 10.1016/j.biomaterials.2012.02.034. [PubMed: 22386919]

(32). Cho D-I; Kim MR; Jeong H; Jeong HC; Jeong MH; Yoon SH; Kim YS; Ahn Y Mesenchymal Stem Cells Reciprocally Regulate the M1/M2 Balance in Mouse Bone Marrow-Derived Macrophages. Exp. Mol. Med 2014, 46 (1), e70–e70. 10.1038/emm.2013.135. [PubMed: 24406319]

(33). Kzhyshkowska J; Gudima A; Riabov V; Dollinger C; Lavalle P; Vrana NE Macrophage Responses to Implants: Prospects for Personalized Medicine. J. Leukoc. Biol 2015, 98 (6), 953–962. 10.1189/jlb.5VMR0415-166R. [PubMed: 26168797]

(34). Bougas K; Jimbo R; Xue Y; Mustafa K; Wennerberg A Novel Implant Coating Agent Promotes Gene Expression of Osteogenic Markers in Rats during Early Osseointegration. Int. J. Biomater 2012, 2012, 1–9. 10.1155/2012/579274.

(35). Vishwakarma A; Bhise NS; Evangelista MB; Rouwkema J; Dokmeci MR; Ghaemmaghami AM; Vrana NE; Khademhosseini A Engineering Immunomodulatory Biomaterials To Tune the Inflammatory Response. Trends Biotechnol. 2016, 34 (6), 470–482. 10.1016/j.tibtech.2016.03.009. [PubMed: 27138899]

(36). Hotchkiss KM; Reddy GB; Hyzy SL; Schwartz Z; Boyan BD; Olivares-Navarrete R Titanium Surface Characteristics, Including Topography and Wettability, Alter Macrophage Activation. Acta Biomater. 2016, 31, 425–434. 10.1016/j.actbio.2015.12.003. [PubMed: 26675126]

(37). Lee RSB; Hamlet SM; Ivanovski S The Influence of Titanium Surface Characteristics on Macrophage Phenotype Polarization during Osseous Healing in Type I Diabetic Rats: A

Pilot Study. Clin. Oral Implants Res 2017, 28 (10), e159–e168. 10.1111/clr.12979. [PubMed: 27637574]

(38). Spriano S; Yamaguchi S; Baino F; Ferraris S A Critical Review of Multifunctional Titanium Surfaces: New Frontiers for Improving Osseointegration and Host Response, Avoiding Bacteria Contamination. Acta Biomater. 2018, 79, 1–22. 10.1016/j.actbio.2018.08.013. [PubMed: 30121373]

(39). Ma QL; Zhao LZ; Liu RR; Jin BQ; Song W; Wang Y; Zhang YS; Chen LH; Zhang YM Improved Implant Osseointegration of a Nanostructured Titanium Surface via Mediation of Macrophage Polarization. Biomaterials 2014, 35 (37), 9853–9867. 10.1016/j.biomaterials.2014.08.025. [PubMed: 25201737]

(40). Ma A; You Y; Chen B; Wang W; Liu J; Qi H; Liang Y; Li Y; Li C Icariin/Aspirin Composite Coating on TiO2 Nanotubes Surface Induce Immunomodulatory Effect of Macrophage and Improve Osteoblast Activity. Coatings 2020, 10 (4), 427. 10.3390/coatings10040427.

(41). Zhang R; Liu X; Xiong Z; Huang Q; Yang X; Yan H; Ma J; Feng Q; Shen Z The Immunomodulatory Effects of Zn-Incorporated Micro/Nanostructured Coating in Inducing Osteogenesis. Artif. Cells, Nanomedicine Biotechnol 2018, 46 (sup1), 1123–1130. 10.1080/21691401.2018.1446442.

(42). Liu R; Chen S; Huang P; Liu G; Luo P; Li Z; Xiao Y; Chen Z; Chen Z Immunomodulation-Based Strategy for Improving Soft Tissue and Metal Implant Integration and Its Implications in the Development of Metal Soft Tissue Materials. Adv. Funct. Mater 2020, 30 (21), 1910672. 10.1002/adfm.201910672.

(43). Guida L; Oliva A; Basile MA; Giordano M; Nastri L; Annunziata M Human Gingival Fibroblast Functions Are Stimulated by Oxidized Nano-Structured Titanium Surfaces. J. Dent 2013, 41 (10), 900–907. 10.1016/j.jdent.2013.07.009. [PubMed: 23907085]

(44). Gindri IM; Palmer KL; Siddiqui DA; Aghyarian S; Frizzo CP; Martins MAP; Rodrigues DC Evaluation of Mammalian and Bacterial Cell Activity on Titanium Surface Coated with Dicationic Imidazolium-Based Ionic Liquids. RSC Adv. 2016, 6 (43), 36475–36483. 10.1039/C6RA01003B.

(45). Miura S; Takebe J Biological Behavior of Fibroblast-like Cells Cultured on Anodized-Hydrothermally Treated Titanium with a Nanotopographic Surface Structure. J. Prosthodont. Res 2012, 56 (3), 178–186. 10.1016/j.jpor.2011.11.004. [PubMed: 22264674]

(46). McNally AK; Anderson JM Phenotypic Expression in Human Monocyte-Derived Interleukin-4-Induced Foreign Body Giant Cells and Macrophages in Vitro: Dependence on Material Surface Properties. J. Biomed. Mater. Res. - Part A 2015, 103 (4), 1380–1390. 10.1002/jbm.a.35280.

(47). Visai L; de Nardo L; Punta C; Melone L; Cigada A; Imbriani M; Arciola CR Titanium Oxide Antibacterial Surfaces in Biomedical Devices. Int. J. Artif. Organs 2011, 34 (9), 929–946. 10.5301/ijao.5000050. [PubMed: 22094576]

(48). Scislowska-Czarnecka A; Menaszek E; Szaraniec B; Kolaczkowska E Ceramic Modifications of Porous Titanium: Effects on Macrophage Activation. Tissue Cell 2012, 44 (6), 391–400. 10.1016/j.tice.2012.08.002. [PubMed: 22939219]

(49). Vallés G; Gil-Garay E; Munuera L; Vilaboa N Modulation of the Cross-Talk between Macrophages and Osteoblasts by Titanium-Based Particles. Biomaterials 2008, 29 (15), 2326–2335. 10.1016/j.biomaterials.2008.02.011. [PubMed: 18313744]

(50). Alfarsi MA; Hamlet SM; Ivanovski S Titanium Surface Hydrophilicity Modulates the Human Macrophage Inflammatory Cytokine Response. J. Biomed. Mater. Res. - Part A 2014, 102 (1), 60–67. 10.1002/jbm.a.34666.

(51). Hamlet S; Alfarsi M; George R; Ivanovski S The Effect of Hydrophilic Titanium Surface Modification on Macrophage Inflammatory Cytokine Gene Expression. Clin. Oral Implants Res 2012, 23 (5), 584–590. 10.1111/j.1600-0501.2011.02325.x. [PubMed: 22093029]

(52). Hough WL; Smiglak M; Rodríguez H; Swatloski RP; Spear SK; Daly DT; Pernak J; Grisel JE; Carliss RD; Soutullo MD; Davis JH Jr.; Rogers RD; Vandrovcová M; Bačáková L Adhesion, Growth and Differentiation of Osteoblasts on Surface-Modified Materials Developed for Bone Implants. Physiol. Res 2011, 60 (3), 403–417. 10.1039/b706677p. [PubMed: 21401307]

(53). Zhao B; Van Der Mei HC; Subbiahdoss G Soft Tissue Integration versus Early Biofilm Formation on Different Dental Implant Materials. Dent. Mater 2014, 30 (7), 716–727. 10.1016/j.dental.2014.04.001. [PubMed: 24793200]

(54). Pérez-Tanoira R; Han X; Soininen A; Aarnisalo AA; Tiainen VM; Eklund KK; Esteban J; Kinnari TJ Competitive Colonization of Prosthetic Surfaces by Staphylococcus Aureus and Human Cells. J. Biomed. Mater. Res. - Part A 2017, 105 (1), 62–72. 10.1002/jbm.a.35863.

(55). Gristina AG; Naylor P; Myrvik Q Infections from Biomaterials and Implants: A Race for the Surface. Med. Prog. Technol 1989, 14 (3–4), 205–224.

(56). Gahlert M; Roehling S; Sprecher CM; Kniha H; Milz S; Bormann K In Vivo Performance of Zirconia and Titanium Implants: A Histomorphometric Study in Mini Pig Maxillae. Clin. Oral Implants Res 2012, 23 (3), 281–286. 10.1111/j.1600-0501.2011.02157.x. [PubMed: 21806681]

(57). Fenner M; Vairaktaris E; Fischer K; Schlegel KA; Neukam FW; Nkenke E Influence of Residual Alveolar Bone Height on Osseointegration of Implants in the Maxilla: A Pilot Study. Clin. Oral Implants Res 2009, 20 (6), 555–559. 10.1111/j.1600-0501.2008.01598.x. [PubMed: 19515034]

(58). Caneva M; Salata LA; De Souza SS; Baffone G; Lang NP; Botticelli D Influence of Implant Positioning in Extraction Sockets on Osseointegration: Histomorphometric Analyses in Dogs. Clin. Oral Implants Res 2010, 21 (1), 43–49. 10.1111/j.1600-0501.2009.01842.x. [PubMed: 20070746]

(59). Favero R; Lang NP; Salata LA; Neto ECM; Caroprese M; Botticelli D Sequential Healing Events of Osseointegration at UnicCa® and SLActive® Implant Surfaces: An Experimental Study in the Dog. Clin. Oral Implants Res 2016, 27 (2), 203–210. 10.1111/clr.12591. [PubMed: 25818234]

(60). Philipp A; Duncan W; Roos M; Hämmerle CH; Attin T; Schmidlin PR Comparison of SLA® or SLActive® Implants Placed in the Maxillary Sinus with or without Synthetic Bone Graft Materials - An Animal Study in Sheep. Clin. Oral Implants Res 2014, 25 (10), 1142–1148. 10.1111/clr.12255. [PubMed: 24112524]

(61). Kolonidis SG; Renvert S; Hammerle CHF; Lang NP; Harris D; Claffey N Osseointegration on Implant Surfaces Previously Contaminated with Plaque. An Experimental Study in the Dog. Clin. Oral Implants Res 2003, 14 (4), 373–380. 10.1034/j.1600-0501.2003.01871.x. [PubMed: 12868999]

(62). Persson LG; Araujo MG; Berglundh T; Grondahl K; Lindhe J Resolution of Peri-Implantitis Following Treatment. An Experimental Study in the Dog. Clin. Oral Implants Res 1999, 10 (3), 195–203. 10.1034/j.1600-0501.1999.100302.x. [PubMed: 10522179]

(63). Ou KL; Hsu HJ; Sen Yang T; Lin YH; Chen CS; Peng PW Osseointegration of Titanium Implants with SLAffinity Treatment: A Histological and Biomechanical Study in Miniature Pigs. Clin. Oral Investig 2016, 20 (7), 1515–1524. 10.1007/s00784-015-1629-7.

(64). Apostu D; Lucaciu O; Mester A; Oltean-Dan D; Gheban D; Rares Ciprian Benea H Tibolone, Alendronate, and Simvastatin Enhance Implant Osseointegration in a Preclinical in Vivo Model. Clin. Oral Implants Res 2020, 31 (7), 655–668. 10.1111/clr.13602. [PubMed: 32279374]

(65). Omar O; Lennerås M; Svensson S; Suska F; Emanuelsson L; Hall J; Nannmark U; Thomsen P Integrin and Chemokine Receptor Gene Expression in Implant-Adherent Cells during Early Osseointegration. J. Mater. Sci. Mater. Med 2010, 21 (3), 969–980. 10.1007/s10856-009-3915-x. [PubMed: 19856201]

(66). Thalji G; Gretzer C; Cooper LF Comparative Molecular Assessment of Early Osseointegration in Implant-Adherent Cells. Bone 2013, 52 (1), 444–453. 10.1016/j.bone.2012.07.026. [PubMed: 22884725]

(67). Omar OM; Lennerås ME; Suska F; Emanuelsson L; Hall JM; Palmquist A; Thomsen P The Correlation between Gene Expression of Proinflammatory Markers and Bone Formation during Osseointegration with Titanium Implants. Biomaterials 2011, 32 (2), 374–386. 10.1016/j.biomaterials.2010.09.011. [PubMed: 20933278]

(68). Allen MR; Burr DB Bone Cells. In Basic and Applied Bone Biology; 2019; p 53. 10.1016/B978-0-12-416015-6.00004-6.

(69). Du Z; Lee RSB; Hamlet S; Doan N; Ivanovski S; Xiao Y Evaluation of the First Maxillary Molar Post-Extraction Socket as a Model for Dental Implant Osseointegration Research. Clin. Oral Implants Res 2016, 27 (12), 1469–1478. 10.1111/clr.12571. [PubMed: 25694130]

(70). Nagasawa M; Takano R; Maeda T; Uoshima K Observation of the Bone Surrounding an Overloaded Implant in a Novel Rat Model. Int. J. Oral Maxillofac. Implants 2013, 28 (1), 109–116. 10.11607/jomi.2388. [PubMed: 23377055]

(71). Imai Y; Yokoyama A; Yamamoto S; Obata T; Iizuka T; Kohgo T; Shindoh M Peri-Implant Tissue after Osseointegration in Diabetes in Rat Maxilla. J. Oral Biosci 2006, 48 (1), 54–61. 10.1016/s1349-0079(06)80019-8.

(72). Fujii N; Kusakari H; Maeda T A Histological Study on Tissue Responses to Titanium Implantation in Rat Maxilla: The Process of Epithelial Regeneration and Bone Reaction. J. Periodontol 1998, 69 (4), 485–495. 10.1902/jop.1998.69.4.485. [PubMed: 9609380]

(73). Ikeda Y; Hasegawa T; Yamamoto T; de Freitas PHL; Oda K; Yamauchi A; Yokoyama A Histochemical Examination on the Peri-Implant Bone with Early Occlusal Loading after the Immediate Placement into Extraction Sockets. Histochem. Cell Biol 2018, 149 (4), 433–447. 10.1007/s00418-018-1644-2. [PubMed: 29435764]

(74). Shirakura M; Fujii N; Ohnishi H; Taguchi Y; Ohshima H; Nomura S; Maeda T Tissue Response to Titanium Implantation in the Rat Maxilla, with Special Reference to the Effects of Surface Conditions on Bone Formation. Clin. Oral Implants Res 2003, 14 (6), 687–696. 10.1046/j.0905-7161.2003.00960.x. [PubMed: 15015943]

(75). Haga M; Fujii N; Nozawa-Inoue K; Nomura S; Oda K; Uoshima K; Maeda T Detailed Process of Bone Remodeling after Achievement of Osseointegration in a Rat Implantation Model. Anat. Rec 2009, 292 (1), 38–47. 10.1002/ar.20748.

(76). Lin Z; Rios HF; Volk SL; Sugai JV; Jin Q; Giannobile WV Gene Expression Dynamics During Bone Healing and Osseointegration. J. Periodontol 2011, 82 (7), 1007–1017. 10.1902/jop.2010.100577. [PubMed: 21142982]

(77). Hou X; Weiler MA; Winger JN; Morris JR; Borke JL Rat Model for Studying Tissue Changes Induced by the Mechanical Environment Surrounding Loaded Titanium Implants. Int. J. Oral Maxillofac. Implants 2020, 24 (5), 800–807.

(78). Giro G; Coelho PG; Sales-Pessoa R; Rodrigues Pereira RM; Kawai T; Perez Orrico SR Influence of Estrogen Deficiency on Bone around Osseointegrated Dental Implants: An Experimental Study in the Rat Jaw Model. J. Oral Maxillofac. Surg 2011, 69 (7), 1911–1918. 10.1016/j.joms.2011.01.028. [PubMed: 21530046]

(79). Park S; Heo H-A; Min J-S; Pyo S-W Effect of Raloxifene on Bone Formation Around Implants in the Osteoporotic Rat Maxilla: Histomorphometric and Microcomputed Tomographic Analysis. Int. J. Oral Maxillofac. Implants 2020, 35 (2), 249–256. 10.11607/jomi.7811. [PubMed: 32142560]

(80). Du Z; Xiao Y; Hashimi S; Hamlet SM; Ivanovski S The Effects of Implant Topography on Osseointegration under Estrogen Deficiency Induced Osteoporotic Conditions: Histomorphometric, Transcriptional and Ultrastructural Analysis. Acta Biomater. 2016, 42, 351–363. 10.1016/j.actbio.2016.06.035. [PubMed: 27375286]

(81). Dunn CA; Jin Q; Taba M; Franceschi RT; Bruce Rutherford R; Giannobile WV BMP Gene Delivery for Alveolar Bone Engineering at Dental Implant Defects. Mol. Ther 2005, 11 (2), 294–299. 10.1016/j.ymthe.2004.10.005. [PubMed: 15668141]

(82). Freire MO; Sedghizadeh PP; Schaudinn C; Gorur A; Downey JS; Choi J-H; Chen W; Kook J-K; Chen C; Goodman SD; Zadeh HH Development of an Animal Model for Aggregatibacter Actinomycetemcomitans Biofilm-Mediated Oral Osteolytic Infection: A Preliminary Study. J. Periodontol 2011, 82 (5), 778–789. 10.1902/jop.2010.100263. [PubMed: 21222546]

(83). Barros e Lima Bueno R; Dias AP; Ponce KJ; Brunski JB; Nanci A System for Application of Controlled Forces on Dental Implants in Rat Maxillae: Influence of the Number of Load Cycles on Bone Healing. J. Biomed. Mater. Res. Part B Appl. Biomater 2020, 108 (3), 965–975. 10.1002/jbm.b.34449.

(84). Yue G; Edani H; Sullivan A; Jiang S; Kazerani H; Saghiri MA Is Maxillary Diastema an Appropriate Site for Implantation in Rats? Int. J. Implant Dent 2020, 6 (1), 8. 10.1186/s40729-019-0203-5. [PubMed: 32100121]

(85). Viera-Negrón YE; Ruan W; Winger JN; Hou X; Sharawy MM; Borke JL Effect of Ovariectomy and Alendronate on Implant Osseointegration in Rat Maxillary Bone. J. Oral Implantol 2008, 34 (2), 76–82. 10.1563/1548-1336(2008)34[76:EOOAAO]2.0.CO;2. [PubMed: 18478902]

(86). Karimbux NY; Sirakian A; Weber HP; Nishimura I A New Animal Model for Molecular Biological Analysis of the Implant-Tissue Interface: Spatial Expression of Type XII Collagen MRNA around a Titanium Oral Implant. J. Oral Implantol 1995, 21 (2), 107–113; discussion 114-5. [PubMed: 8699501]

(87). de Siqueira CRB; Semenoff TADV; Palma VC; Borges ÁH; da Silva NF; Segundo AS Effect of Chronic Stress on Implant Osseointegration into Rat's Mandible. Acta Cir. Bras 2015, 30 (9), 598–603. 10.1590/S0102-865020150090000003. [PubMed: 26465103]

(88). Biguetti CC; Cavalla F; Silveira EM; Fonseca AC; Vieira AE; Tabanez AP; Rodrigues DC; Trombone APF; Garlet GP Oral Implant Osseointegration Model in C57Bl/6 Mice: Microtomographic, Histological, Histomorphometric and Molecular Characterization. J. Appl. Oral Sci 2018, 26. 10.1590/1678-7757-2017-0601.

(89). Mouraret S; Hunter DJ; Bardet C; Brunski JB; Bouchard P; Helms JA A Pre-Clinical Murine Model of Oral Implant Osseointegration. Bone 2014, 58, 177–184. 10.1016/j.bone.2013.07.021. [PubMed: 23886841]

(90). Albrektsson T; Eriksson AR; Friberg B; Lekholm U; Lindahl L; Nevins M; Oikarinen V; Roos J; Sennerby L; Astrand P Histologic Investigations on 33 Retrieved Nobelpharma Implants. Clin. Mater 1993, 12 (1), 1–9. 10.1016/0267-6605(93)90021-X. [PubMed: 10148779]

(91). Diepenhorst NA; Nowell CJ; Rueda P; Henriksen K; Pierce T; Cook AE; Pastoureau P; Sabatini M; Charman WN; Christopoulos A; Summers RJ; Sexton PM; Langmead CJ High Throughput, Quantitative Analysis of Human Osteoclast Differentiation and Activity. Anal. Biochem 2017, 519, 51–56. 10.1016/j.ab.2016.12.010. [PubMed: 27988276]

(92). Carter LE; Kilroy G; Gimble JM; Floyd ZE An Improved Method for Isolation of RNA from Bone. BMC Biotechnol. 2012, 12 (1), 5. 10.1186/1472-6750-12-5. [PubMed: 22260224]

(93). Albrektsson T; Eriksson AR; Friberg B; Lekholm U; Lindahl L; Nevins M; Oikarinen V; Roos J; Sennerby L; Astrand P Histologic Investigations on 33 Retrieved Nobelpharma Implants. Clin. Mater 1993, 12 (1), 1–9. 10.1016/0267-6605(93)90021-X. [PubMed: 10148779]

(94). Trindade R; Albrektsson T; Tengvall P; Wennerberg A Foreign Body Reaction to Biomaterials: On Mechanisms for Buildup and Breakdown of Osseointegration. Clin. Implant Dent. Relat. Res 2016, 18 (1), 192–203. 10.1111/cid.12274. [PubMed: 25257971]

(95). Kyriakides TR; Foster MJ; Keeney GE; Tsai A; Giachelli CM; Clark-Lewis I; Rollins BJ; Bornstein P The CC Chemokine Ligand, CCL2/MCP1, Participates in Macrophage Fusion and Foreign Body Giant Cell Formation. Am. J. Pathol 2004, 165 (6), 2157–2166. 10.1016/S0002-9440(10)63265-8. [PubMed: 15579457]

(96). Ambarus CA; Krausz S; van Eijk M; Hamann J; Radstake TRDJ; Reedquist KA; Tak PP; Baeten DLP Systematic Validation of Specific Phenotypic Markers for in Vitro Polarized Human Macrophages. J. Immunol. Methods 2012, 375 (1–2), 196–206. 10.1016/j.jim.2011.10.013. [PubMed: 22075274]

(97). Xue Q; Yan Y; Zhang R; Xiong H Regulation of INOS on Immune Cells and Its Role in Diseases. Int. J. Mol. Sci 2018, 19 (12), 3805. 10.3390/ijms19123805.

(98). Yu T; Wang W; Nassiri S; Kwan T; Dang C; Liu W; Spiller KL Temporal and Spatial Distribution of Macrophage Phenotype Markers in the Foreign Body Response to Glutaraldehyde-Crosslinked Gelatin Hydrogels. J. Biomater. Sci. Polym. Ed 2016, 27 (8), 721–742. 10.1080/09205063.2016.1155881. [PubMed: 26902292]

(99). Hotchkiss KM; Sowers KT; Olivares-Navarrete R Novel in Vitro Comparative Model of Osteogenic and Inflammatory Cell Response to Dental Implants. Dent. Mater 2019, 35 (1), 176–184. 10.1016/j.dental.2018.11.011. [PubMed: 30509481]

(100). Etzerodt A; Moestrup SK CD163 and Inflammation: Biological, Diagnostic, and Therapeutic Aspects. Antioxid. Redox Signal 2013, 18 (17), 2352–2363. 10.1089/ars.2012.4834. [PubMed: 22900885]

(101). Ivanovski S; Hamlet S; Salvi GE; Huynh-Ba G; Bosshardt DD; Lang NP; Donos N Transcriptional Profiling of Osseointegration in Humans. Clin. Oral Implants Res 2011, 22 (4), 373–381. 10.1111/j.1600-0501.2010.02112.x. [PubMed: 21561479]

(102). Aoe S; Takada Y Regulation of Bone Metabolism. In Reports of Biochemistry and Molecular Biology; 2005; pp 317–334. 10.1201/9781420028836.ch14.

(103). Knowles HJ; Athanasou NA Canonical and Non-Canonical Pathways of Osteoclast Formation. Histol. Histopathol 2009, 24 (3), 337–346. 10.14670/HH-24.337. [PubMed: 19130404]

(104). Trindade R; Albrektsson T; Galli S; Prgomet Z; Tengvall P; Wennerberg A Osseointegration and Foreign Body Reaction: Titanium Implants Activate the Immune System and Suppress Bone Resorption during the First 4 Weeks after Implantation. Clin. Implant Dent. Relat. Res 2018, 20 (1), 82–91. 10.1111/cid.12578. [PubMed: 29283206]

(105). Anitua E; Andia I; Ardanza B; Nurden P; Nurden A Autologous Platelets as a Source of Proteins for Healing and Tissue Regeneration. Thromb. Haemost 2004, 91 (01), 4–15. 10.1160/TH03-07-0440. [PubMed: 14691563]

(106). Ferrara N; Gerber H-P; LeCouter J The Biology of VEGF and Its Receptors. Nat. Med 2003, 9 (6), 669–676. 10.1038/nm0603-669. [PubMed: 12778165]

(107). Allen MR; Burr DB Local Regulation of Bone Cell Function. In Basic and Applied Bone Biology; 2019; p 80. 10.1016/B978-0-12-416015-6.00004-6.

(108). Chen G; Deng C; Li Y-P TGF-β and BMP Signaling in Osteoblast Differentiation and Bone Formation. Int. J. Biol. Sci 2012, 8 (2), 272–288. 10.7150/ijbs.2929. [PubMed: 22298955]

(109). CIRANO FR; PIMENTEL SP; RIBEIRO FV; CASATI MZ; CASARIN RC; GALLAFASSI DF; NISHII D; CORRÊA MG Impact of History of Periodontitis on Gene Expression of Bone-Related Factors in Young Patients. Braz. Oral Res 2020, 34. 10.1590/1807-3107bor-2020.vol34.0014.

(110). Benisch P; Schilling T; Klein-Hitpass L; Frey SP; Seefried L; Raaijmakers N; Krug M; Regensburger M; Zeck S; Schinke T; Amling M; Ebert R; Jakob F The Transcriptional Profile of Mesenchymal Stem Cell Populations in Primary Osteoporosis Is Distinct and Shows Overexpression of Osteogenic Inhibitors. PLoS One 2012, 7 (9), e45142. 10.1371/journal.pone.0045142. [PubMed: 23028809]

(111). Fiorellini J; Glindmann S; Salcedo J; Weber H-P; Park C-J; Sarmiento H The Effect of Osteopontin and an Osteopontin-Derived Synthetic Peptide Coating on Osseointegration of Implants in a Canine Model. Int. J. Periodontics Restorative Dent 2016, 36 (6), e88–e94. 10.11607/prd.2830. [PubMed: 27740646]

(112). Galindo-Moreno P; Hernandez-Cortes P; Padial-Molina M; Vizoso ML; Crespo-Lora V; O'Valle F Immunohistochemical Osteopontin Expression in Bone Xenograft in Clinical Series of Maxillary Sinus Lift. J. Oral Sci. Rehabil 2015, 1, 42–50.

(113). Wang J; Zhou H-Y; Salih E; Xu L; Wunderlich L; Gu X; Hofstaetter JG; Torres M; Glimcher MJ Site-Specific In Vivo Calcification and Osteogenesis Stimulated by Bone Sialoprotein. Calcif. Tissue Int 2006, 79 (3), 179–189. 10.1007/s00223-006-0018-2. [PubMed: 16969594]

(114). Sollazzo V; Palmieri A Trabecular Titanium Induces Osteoblastic Bone Marrow Stem Cells Differentiation. J. Biotechnol. Biomater 2011, 01 (01). 10.4172/2155-952X.1000102.

(115). Muï¿½oz-Valle J Molecular Modulation of Osteocalcin and Its Relevance in Diabetes (Review). Int. J. Mol. Med 2011. 10.3892/ijmm.2011.706.

(116). Liu J; Nam HK; Campbell C; da S. Gasque KC; Millán JL; Hatch NE Tissue-Nonspecific Alkaline Phosphatase Deficiency Causes Abnormal Craniofacial Bone Development in the Alpl−/− Mouse Model of Infantile Hypophosphatasia. Bone 2014, 67, 81–94. 10.1016/j.bone.2014.06.040. [PubMed: 25014884]

(117). He G; George A Dentin Matrix Protein 1 Immobilized on Type I Collagen Fibrils Facilitates Apatite Deposition in Vitro. J. Biol. Chem 2004, 279 (12), 11649–11656. 10.1074/jbc.M309296200. [PubMed: 14699165]

(118). Du Z; Steck R; Doan N; Woodruff MA; Ivanovski S; Xiao Y Estrogen Deficiency-Associated Bone Loss in the Maxilla: A Methodology to Quantify the Changes in the Maxillary Intra-Radicular Alveolar Bone in an Ovariectomized Rat Osteoporosis Model. Tissue Eng. - Part C Methods 2015, 21 (5), 458–466. 10.1089/ten.tec.2014.0268. [PubMed: 25315176]

(119). Botticelli D; Lang NP Dynamics of Osseointegration in Various Human and Animal Models - a Comparative Analysis. Clin. Oral Implants Res 2017, 28 (6), 742–748. 10.1111/clr.12872. [PubMed: 27214566]

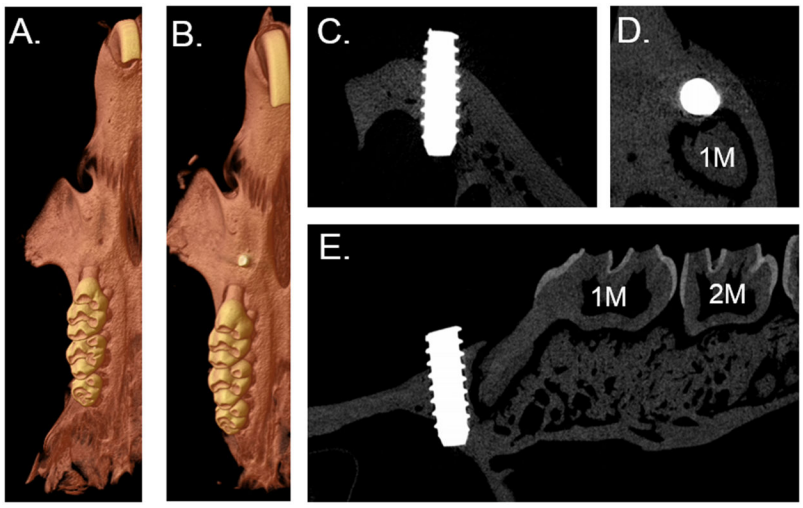

Figure 1.

Placement of cpTi screw into edentulous alveolar crest (EAC). **A.** 3D microtomographic reconstruction of rat maxilla without implant; **B**. 3D microtomographic reconstruction of rat maxilla with implant in EAC; **C**. Transaxial; **D**. Coronal; and **E.** Sagittal radiographs of implant in EAC, 1M and 2M are maxillary first and second molar, respectively.

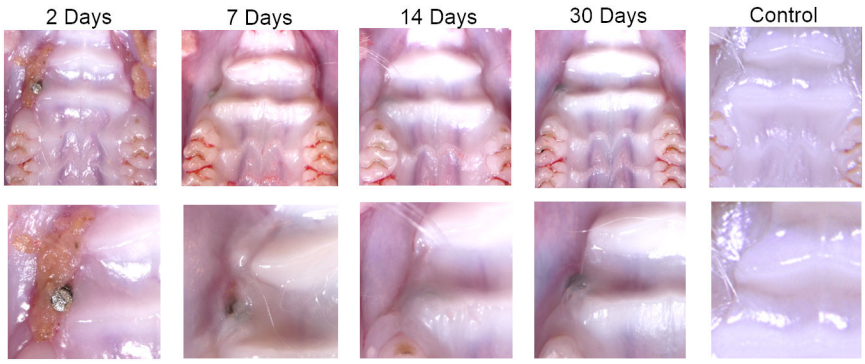

Figure 2.
OM images of mucosal healing post-implantation over time. Left maxilla side contains Ti implant, right maxilla side contains surgical sham.

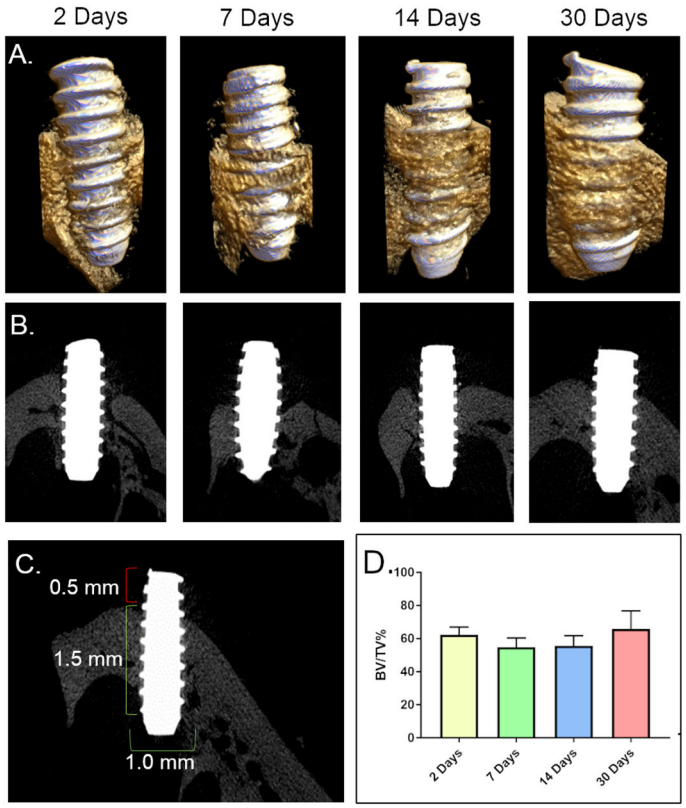

Figure 3.

Microtomographic analysis of bone volume growth. **A**. 3D reconstruction and **B**. Radiographs of bone growth from 2 to 30 days post implantation. **C.** Bone morphometry analysis parameters and **D.** Bone volume / tissue volume % over time.

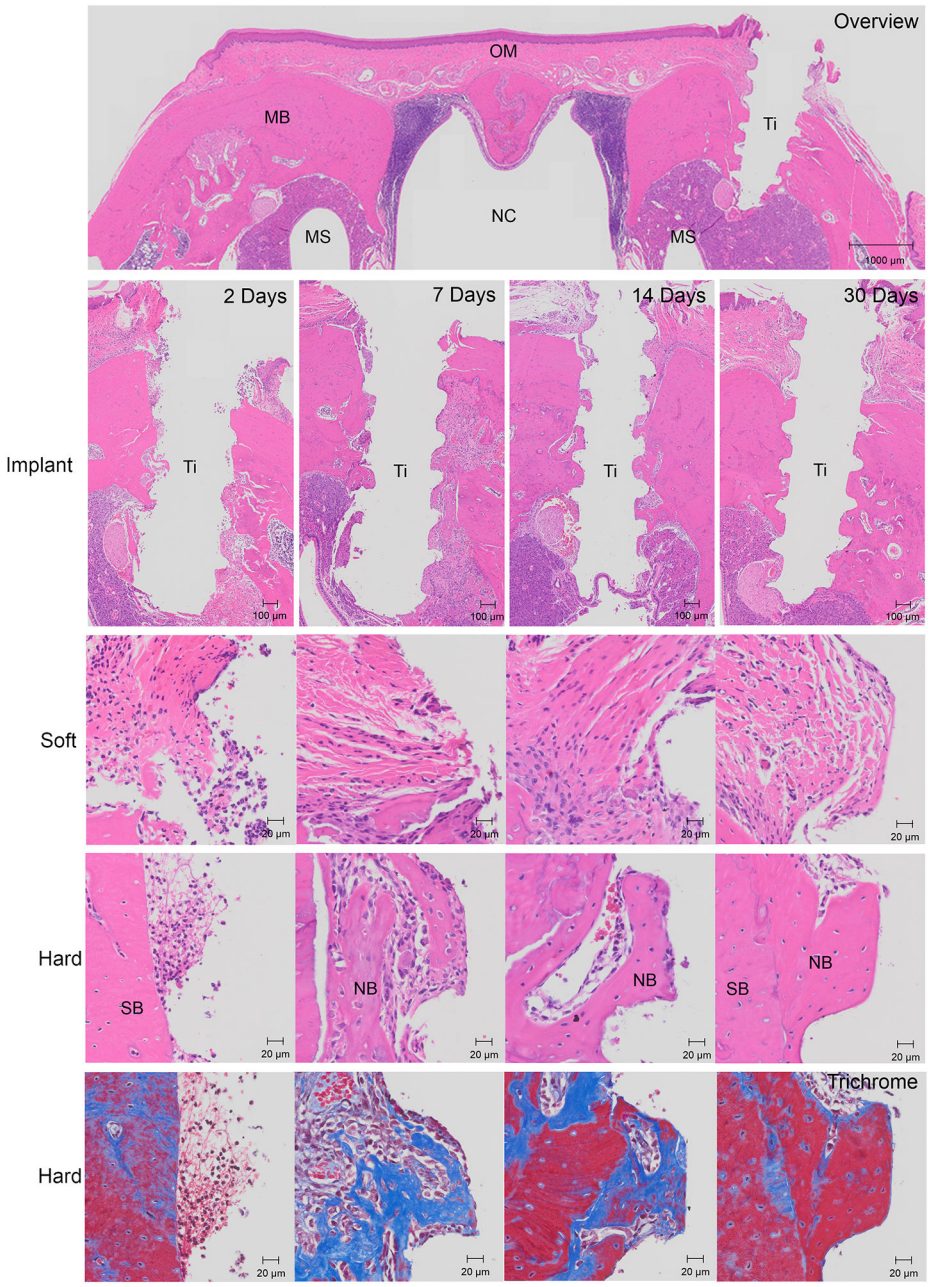

Figure 4.

Histology representing healing panel of maxilla implantation over time, H&E and Masson's Trichrome. Overview panel displays a transaxial view of entire maxilla: MB is maxillary bone, MS is maxillary sinus, NC is nasal cavity, OM is oral mucosa, Ti is void left by titanium implant after processing. Implant panel displays healing over time of both bone and soft tissue adjacent to the implant. Soft and hard tissue panels display a more detailed histology of healing at their respective level: SB is supporting bone, NB is new bone.

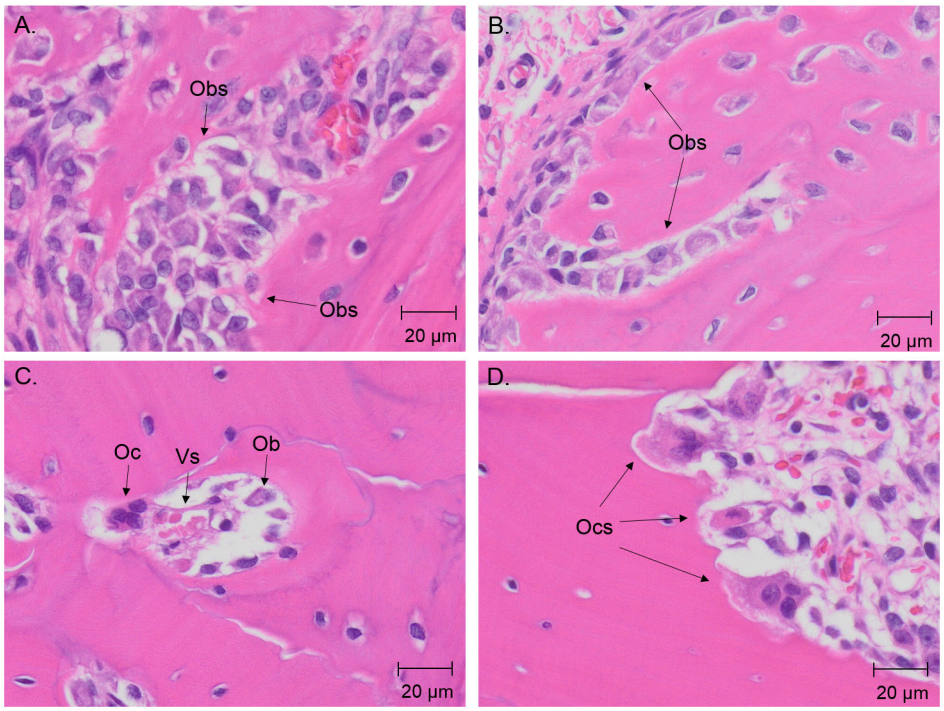

Figure 5.

Histology representing detailed bone-remodeling phenomena, H&E. A-B. Large density of osteoblasts (Obs) present forming new bone at 7 days. C. Basic bone remodeling unit of osteoclast (Oc), osteoblast (Ob) and blood vessel (Vs) present at 14 days. D. Multiple osteoclasts (Ocs) resorbing supporting bone at 7 days.

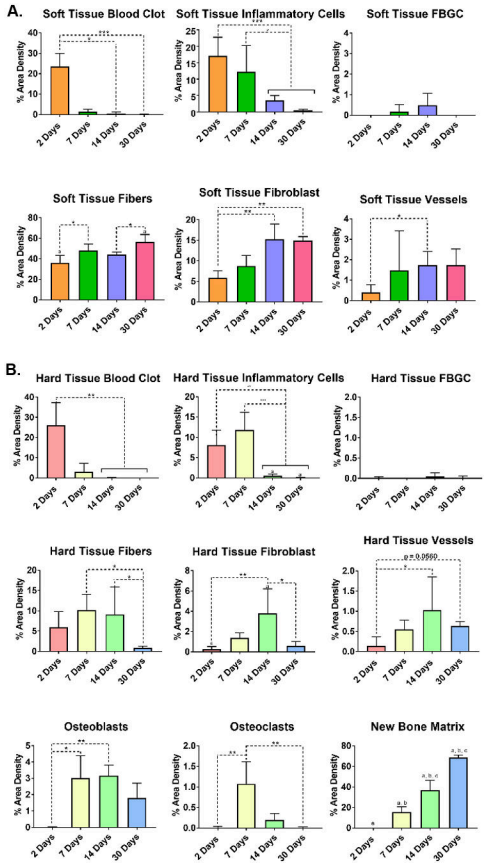

Figure 6.

Histomorphometry of A. Soft tissue and B. Hard tissue healing parameters over time. *, a, b, and c indicates statistical significance between specified groups ($p < 0.05$). ** and *** indicates significance of $p < 0.01$ and $p < 0.001$ respectively.

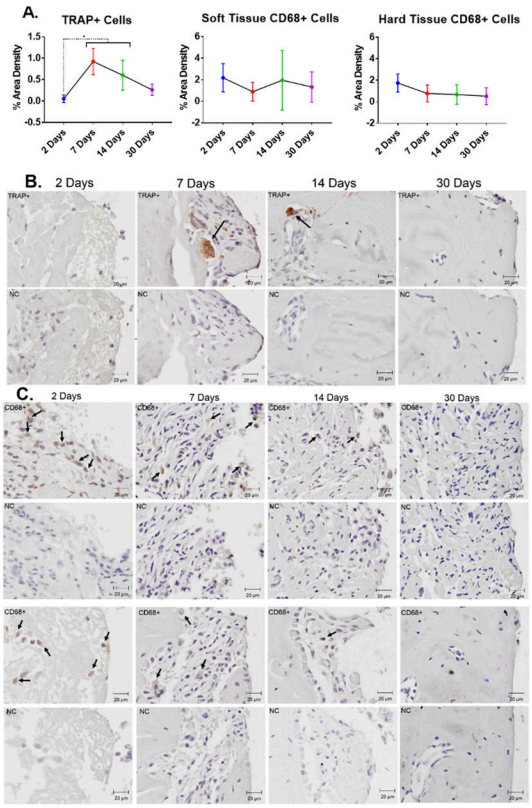

Figure 7.

Immunohistochemistry of osteoclasts and macrophages using CD68 and TRAP. **A**. Histomorphomtery of TRAP+ and CD68+ positive cells in hard and soft tissue over time. .* indicates statistical significance between groups ($p < 0.05$). B. Peri-implant images of TRAP and **C.** CD68 stained tissue with corresponding negative control (NC) over time. Arrows indicate positively marked cells.

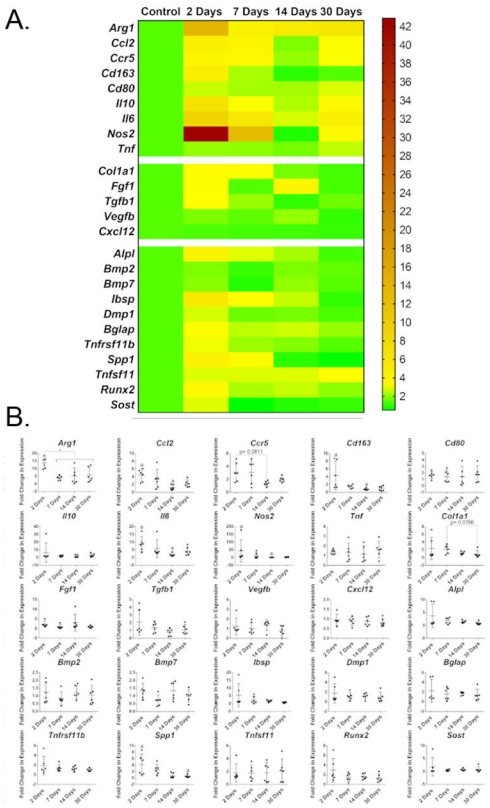

Figure 8.

Fold change in gene expression of peri-implant tissue over time relative to non-surgery control tissue. **A.** Heat map displaying average fold change of inflammatory, tissue reconstruction, and bone remodeling markers **B.** Scatter plot displaying dispersion of gene expression of each marker with 95% CI in peri-implant tissue over time (n=6). * and **a** indicate statistical significance among groups ($p < 0.05$).